Predicting the Soluble Solids Concentration and Acid Ascorbic of Intact Jackfruit var. Tekam Yellow Using Visible Near Infrared Spectroscopy: Effect of Rind and Flesh

Kok Jeng Lim

limkokjeng@gmail.com

Universiti Putra Malaysia

Phebe Ding

Universiti Putra Malaysia

Nazmi Mat Nawi

Universiti Putra Malaysia

Mashitah Jusoh

Universiti Putra Malaysia

Najidah Abdullah

Universiti Putra Malaysia

Siti Saripa Rabiah Mat Lazim

Universiti Putra Malaysia

Research Article

Keywords: Bronzing disease, Pantoea stewartii, visible near-infrared spectroscopy (Vis-NIRS), partial least squares regression (PLSR), non-destructive prediction

Posted Date: January 8th, 2026

DOI: https://doi.org/10.21203/rs.3.rs-8272009/v1

Additional Declarations: No competing interests reported.

Predicting the Soluble Solids Concentration and Acid Ascorbic of Intact Jackfruit var. Tekam Yellow Using Visible Near Infrared Spectroscopy: Effect of Rind and Flesh

Running Title

Vis–NIR Prediction of Jackfruit SSC and AA

Kok Jeng Lim[1*], Phebe Ding[1], Nazmi Mat Nawi[2,3], Mashitah Jusoh[1], Najidah Abdullah[2,3] and Siti Saripa Rabiah Mat Lazim[3]

[1]Department of Crop Science, Faculty of Agriculture, Universiti Putra Malaysia, 43400 UPM Serdang, Selangor Malaysia.
[2]Department of Biological and Agricultural Engineering, Faculty of Engineering, Universiti Putra Malaysia, 43400 UPM Serdang, Selangor, Malaysia.
[3]Institute of Plantation Studies, Universiti Putra Malaysia, 43400 UPM Serdang, Selangor, Malaysia.

Email addresses:
limkokjeng@gmail.com (Kok Jeng Lim)
phebe@upm.edu.my (Phebe Ding)
nazmimat@upm.edu.my (Nazmi Mat Nawi)
mashitahj@upm.edu.my (Mashitah Jusoh)
najidahabdullah7@gmail.com (Najidah Abdullah)
sariparabiahmatlazim@gmail.com (Siti Saripa Rabiah Mat Lazim)
*Corresponding author

List of Table/Figure

Table = 8
Figure = 27 (24 in colour, 3 in black & white)

Predicting the Soluble Solids Concentration and Acid Ascorbic of Intact Jackfruit var. Tekam Yellow Using Visible Near Infrared Spectroscopy: Effect of Rind and Flesh

Abstract

The Malaysian jackfruit (*Artocarpus heterophyllus* cv. Tekam Yellow) industry faces a major challenge from *jackfruit bronzing*, a physiological disorder caused by *Pantoea stewartii* subsp. *stewartii*. The disease induces internal discoloration of the flesh and rag from yellowish-orange to reddish hues, while the rind remains visually unaffected, hindering early detection and reducing market value. This study assessed the potential of visible–near infrared spectroscopy (Vis–NIRS) as a non-destructive diagnostic tool for detecting internal bronzing through rind spectral analysis at 10, 12, and 14 weeks after anthesis (WAA). Fifty-four syncarps were sampled, and reflectance spectra (500–950 nm) from 30 rind sections per fruit were recorded using an Ocean Optics HR4000 spectrometer. Partial Least Squares Regression (PLSR) models were developed to predict soluble solids concentration (SSC) and ascorbic acid (AA) using pre-processed spectra (Savitzky–Golay smoothing, Standard Normal Variate, and Multiplicative Scatter Correction). The optimal models achieved high validation performance with Rv^2 values of 0.94–0.97 and RMSEV of 1.26–1.67% for SSC and 0.72–1.59 mg/100 g for AA. Reference analyses indicated mean SSC values of 4.38%, 9.09%, and 10.01%, and AA contents of 18.98, 19.95, and 12.24 mg/100 g at 10, 12, and 14 WAA, respectively. ANOVA and Fisher's LSD ($p \leq 0.05$) confirmed significant variations across maturity stages and disease conditions. These findings demonstrate that Vis–NIRS integrated with chemometric modeling provides a rapid, accurate, and non-invasive method for early bronzing detection and quality assessment in jackfruit supply chains.

Keywords: *Bronzing disease*, *Pantoea stewartii*, visible near-infrared spectroscopy (Vis-NIRS), partial least squares regression (PLSR), non-destructive prediction

1. INTRODUCTION

Jackfruit is a tropical fruit belonging to the Moraceae family, holds significant economic, nutritional, and socio-cultural value across Southeast Asia, including Malaysia. Originating in the rainforests of the Western Ghats in India, jackfruit is extensively cultivated throughout tropical regions, exhibiting diverse utility beyond its edible fruit, including medicinal, industrial, and agroforestry applications (Azad *et al*., 2007; Saxena *et al*., 2011). Jackfruit is increasingly recognized as a commercially important crop due to rising domestic consumption, expanding export markets, and its versatile use in processed food products (Chakraborty *et al*., 2025).

However, recent developments in jackfruit cultivation have introduced significant challenges, particularly concerning the emergence of a new bacterial disease known as bronzing. Caused by the bacterium *Pantoea stewartii* subsp. *stewartii*, a pathogenic member of the Enterobacteriaceae family, this disease significantly threatens jackfruit production, notably affecting the commercially preferred cultivar Tekam Yellow (Abidin *et al.*, 2020; Ibrahim *et al.*, 2020; Zulperi *et al*., 2017). Characteristically, jackfruit bronzing manifests internally through distinctive yellowish-orange to reddish discoloration of the fruit's flesh without apparent external symptoms, consequently reducing the fruit's aesthetic appeal, nutritional quality, and commercial value (Gapasin *et al.*, 2014; Hernández-Morales *et al*., 2017, 2021).

In Malaysia, initial observations of bronzing symptoms appeared as small reddish-brown lesions within the fruit pulp, rapidly escalating to widespread internal discoloration and severe economic losses due to reduced consumer acceptance and rejection from high-value export markets (Abidin *et al.*, 2020; Ibrahim *et al*., 2020). Consequently, there is an urgent need to develop rapid, accurate, and non-destructive methods for early detection and quality assessment of bronzed jackfruit to mitigate market losses and support sustainable agricultural practices.

Traditional fruit quality assessments commonly utilize destructive laboratory techniques that involve tedious chemical analyses and physical inspection, posing significant limitations such as

time consumption, fruit wastage, and unsuitability for large-scale commercial evaluations (Nicolaï *et al*., 2007; Magwaza *et al*., 2014). Recently, non-destructive analytical techniques have gained prominence, providing efficient and sustainable alternatives to destructive methods, facilitating real-time fruit quality evaluation in commercial operations (Mishra *et al*., 2021; Magwaza *et al*., 2014; Cozzolino *et al.*, 2011). Among these, Visible-Near-Infrared Spectroscopy (Vis-NIRS) has emerged as a powerful tool due to its rapidity, precision, and minimal sample preparation, making it particularly suitable for routine quality control in horticultural industries (Huang *et al*., 2025; Cen & He, 2007).

Vis-NIRS operates by measuring the reflectance or absorption characteristics of biological materials across the electromagnetic spectrum, typically between 780 nm and 2500 nm. It provides insight into intrinsic biochemical components such as soluble sugars, organic acids, vitamins, and moisture content, as well as structural characteristics (Bui *et al.*, 2019; Lammertyn *et al*., 2000; Nicolaï *et al*., 2007). Reflectance patterns captured by Vis-NIRS are closely associated with the chemical composition and physical structure of fruit tissues, allowing for the development of predictive chemometric models through multivariate statistical approaches, particularly Partial Least Squares Regression (PLSR) (Bobelyn *et al*., 2010; Clark *et al*., 2004; Fraser *et al*., 2003).

Several studies have successfully utilized Vis-NIRS combined with advanced chemometrics for the non-destructive assessment of internal quality attributes in fruits such as apples (Bobelyn *et al*., 2010), mandarins (Magwaza *et al*., 2014), kiwifruit (Clark *et al*., 2004), and mangoes (Rungpichayapichet *et al*., 2016). These studies demonstrate the robust potential of Vis-NIRS for predicting soluble solids concentration (SSC), acidity, vitamin content, and ripening stage with high precision, highlighting its practicality for commercial-scale fruit quality monitoring. Nevertheless, despite these promising results, literature regarding the application of Vis-NIRS in jackfruit quality assessment—particularly in diagnosing the bronzing disease—remains limited.

Given the significant economic implications of jackfruit bronzing disease in Malaysia, addressing this research gap becomes imperative. Developing accurate, non-destructive methods capable of detecting internal quality deterioration associated with bronzing at various fruit maturation stages could substantially enhance commercial quality control practices, reduce financial losses, and promote proactive disease management (Nicolaï *et al.*, 2007; Mishra *et al.*, 2021).

Therefore, the primary objective of this study was to evaluate the feasibility and effectiveness of using Vis-NIRS, combined with advanced chemometric modeling techniques, to predict the SSC and ascorbic acid (AA) content of jackfruit cv. Tekam Yellow, distinguishing between healthy and bronzed fruit tissues across distinct maturity stages (10, 12, and 14 weeks after anthesis). By rigorously evaluating spectral pretreatment methods and their impacts on predictive accuracy, this study seeks to establish robust Vis-NIRS-based diagnostic models suitable for practical implementation in the Malaysian jackfruit industry, contributing significantly to sustainable postharvest management and market competitiveness.

2. MATERIALS AND METHODS

2.1 Plant Material and Sampling Procedure

Jackfruit (*Artocarpus heterophyllus* Lam.) cultivar Tekam Yellow was sourced from a commercial orchard, Agro BS Sdn. Bhd., Jasin, Melaka, Malaysia. Fruit was systematically harvested at three distinct maturity stages: 10, 12, and 14 weeks after anthesis (WAA). Each maturity stage consisted of 18 fruits, totaling 54 fruits for the entire study. Harvesting was conducted according to standard horticultural practices to minimize mechanical injury. Fruit was immediately transported to the laboratory at Universiti Putra Malaysia (UPM), Serdang, Selangor, within two hours to preserve their physicochemical integrity (Abdullah *et al.*, 2018; Mijin, 2021).

2.2 Spectral Measurements

Reflectance spectra of jackfruit rind and flesh were collected using a Vis-NIR spectrometer (Ocean Optics HR4000, Ocean Optics Inc., Dunedin, Florida, USA), covering the spectral range from 200 nm to 1100 nm with an optical resolution of 0.5 nm. Based on preliminary testing, the optimal wavelength range selected for analysis was narrowed to 500–950 nm to reduce noise and interference from irrelevant spectral regions (Nicolaï *et al*., 2007; Bobelyn *et al*., 2010).

Fruit samples were systematically divided into 30 equal segments, labeled clearly from top to bottom (Figure 1). Reflectance spectra were obtained using diffuse reflectance mode, with a fixed scanning distance of approximately 1.5 cm to maintain consistency and reduce variations caused by scattering effects (Figure 2 and Figure 3). A halogen light source (HL-2000 12VDC 15W,

Ocean Optics Inc., USA) provided stable illumination, and the lamp was alternated every 30 minutes to avoid intensity fluctuations (Nicolaï *et al*., 2007). Prior to spectral acquisition, calibration was performed using a standard white reference tile with approximately 100% reflectivity. Care was taken to maintain the cleanliness of the reference tile throughout measurements (Abdullah *et al*., 2018; Cen & He, 2007).

2.3 Reference Chemical Analysis

2.3.1 Determination of Soluble Solids Concentration (SSC).

Soluble solids concentration (SSC), expressed as °Brix, was determined using a digital refractometer (Model Pal-1, Atago Co., Tokyo, Japan), following the method outlined by Voon *et al.* (2006). Flesh and rind samples (approximately 5 g each) from each segment were homogenized separately with 20 ml distilled water using a high-speed blender (Model MX V2N, National, Malaysia) for 2 minutes. The homogenized solution was filtered through muslin cloth, and two drops of the filtrate were placed on the refractometer prism. Measurements were recorded in triplicate and averaged. Final SSC values were calculated by multiplying the average reading by the dilution factor (five times dilution), as described by Mijin *et al*., (2021).

The fruit was transported to the Laboratory of Postharvest for physiochemical characteristic determination after NIR radiation had been obtained. The flesh and rind of thirty jackfruit segments from the top, middle, and bottom of the syncarp were sliced into small pieces. Each portion's label was compared to the portions that were extracted from the NIR radiation. To prevent water from evaporating after being placed in the container, each piece is wrapped with soft paper.

The soluble solid content was examined according to Voon *et al*., 2006 by using a refractometer (Pal-1, Atago Co., Tokyo, Japan). Five grams of flesh and rind tissues were weighed and blended with 20 ml of distilled water using a high-speed blender (Model MX V2N, National, Malaysia) for 2 minutes and mixture were filtered through muslin cloth into a 50 ml beaker before performing the SSC measurements. Two drops of filtrate were placed on the prism glass of digital refractometer to obtain three replications of reading. The SSC results were expressed as %SSC (Ali *et al*., 2021). Three readings per rind or flesh were recorded in %SSC and the mean was

calculated. The average readings were multiplied by 5 to obtain its original %SSC of the rind and flesh as the filtrate were diluted for five times (Mijin *et al*., 2021).

2.3.2 Determination of Ascorbic Acid (AA) Content.

Before determining ascorbic acid, 3% metaphosphoric acid (HPO_3) and dye solution had to be prepared. A prepared 3-gram HPO_3 solution will be added to 100 milliliters of distilled water. To stop the solution from oxidizing, it will be stored in a refrigerator. To prepare the dye solution, weigh 21 mg (0.021 g) of sodium bicarbonate, dissolve it in 75 ml of distilled water, and then boil it until the sodium bicarbonate is completely dissolved. After that, 50 mg of 2-6-dischlorophenol-indophenol were added to a 100 ml beaker and allowed to dissolve. Up to 100 milliliters of distilled water were added. We'll store the solution in the fridge. Every time it is used, standardization is required (Mijin *et al*., 2021).

Weigh 100 mg (0.1 g) of ascorbic acid and add 99 ml of 3% HPO_3. Weigh 10 ml of the solution and add 90 ml of 3% HPO_3 to standardize the ascorbic acid solution and coloring factor. Next, 5 ml of 3% cold metaphosphoric acid was combined with 5 ml of measured standard ascorbic acid solution. To get a pink colour, the mixture was titrated with the dye solution. For the assessment, the dye mixture will be titrated.

$$\text{Dye factor} = \frac{\mu\text{g acid ascorbic}}{\text{ml of dye (titre)}}$$

$$= \frac{0.5}{\text{ml of dye (titre)}}$$

Ascorbic acid was measured using the dye method (Nielsen, 2024). A high-speed blender (Model MX V2N, National, Malaysia) was used to homogenize a 5-gram sample of jackfruit flesh from 30 sections for one minute. The blender was combined with 20 ml of 3% metaphosphoric acid HPO_3. Muslin cloth was used to filter the mixture before pouring it into a 50 ml beaker. Subsequently, a standardized dye solution (2-6-dischlorophenol-indophenol) will be titrated with 5ml of jackfruit extract until the extract becomes pink and stays that way for 5 seconds. The ascorbic acid amounts will be computed using the following formula after the titration data have been recorded:

$$\text{Ascorbic acid (mg 100 g}^{-1}\text{ FW)} = \frac{\text{Titre x dye factor x volume made up x 100}}{\text{Aliquot of extractt x volume of sample}}$$

2.4 Chemometric and Statistical Analysis

2.4.1. Spectral Data Preprocessing and Chemometric Modeling.

Spectral data were preprocessed using the Unscrambler X 10.3 software (CAMO AS, Oslo, Norway). Seven preprocessing techniques were comparatively evaluated: Multiplicative Scatter Correction (MSC), Standard Normal Variate (SNV), Moving Average, Gaussian Filter, Median Filter, Savitzky-Golay (SG) smoothing, and combined treatments (SG+SNV, SG+MSC) in Figure 4. These preprocessing methods were chosen to reduce spectral noise and baseline shifts, significantly improving the robustness of subsequent chemometric analyses (Nicolaï *et al*., 2007; Cen & He, 2007).

Partial Least Squares Regression (PLSR) was employed as the primary chemometric modeling technique to predict SSC and AA content based on spectral data. For comparative purposes, additional regression methods—including Multiple Linear Regression (MLR), Principal Component Regression (PCR), and Support Vector-Machine Regression (SVR)—were also assessed (Figure 10). For each batch of varying maturity stages, the data was randomly split into 25% of validation model and 75% of calibration model. Predictions on the calibration datasets (n = 1215) representing 75% of the entire datasets (n = 1620) in three maturity stages (10 WAA, 12 WAA, and 14 WAA) were used to create the PLSR calibration model for predicting the quality attributes of bronzing and normal jackfruits. However, using the remaining 25% of validation datasets (n = 405), a validation model was produced. To create a prediction on the calibration set, the ideal number of latent variables (LV) and error estimation of the PLSR models were chosen (Ali *et al*., 2021). With the use of the PLSR models' goodness of fit and predictive power, the root mean squared error (RMSE) and coefficient of determination (R^2) between the observed and predicted values of the physicochemical parameters of the rind and flesh of jackfruit were computed (Ali *et al.*, 2021).

Model performance and predictive accuracy were evaluated using standard statistical metrics, including the coefficient of determination for calibration (R^2c), coefficient of determination for

validation (R^2v), root mean square error of calibration (RMSEC), and root mean square error of validation (RMSEV). Additionally, bias and residual predictive deviation (RPD) were calculated to comprehensively assess model reliability and robustness (Nicolaï *et al*., 2007; Mishra *et al*., 2021). Equations used are as follows:

$$R^2 = \frac{\sum_{i=1}^{n}(\hat{y}i - yi)^2}{\sum_{i=1}^{n}(\hat{y}i - ym)^2} \qquad \text{(Eq. 1)}$$

$$RMSEC = \sqrt{\frac{1}{nc-1}\sum_{i=1}^{nc}(\hat{y}i - yi)^2} \qquad \text{(Eq. 2)}$$

$$RMSEV = \sqrt{\frac{1}{nv-1}\sum_{i=1}^{nv}(\hat{y}i - yi - bias)^2} \qquad \text{(Eq. 3)}$$

Which n is the number of the data sample, n_c is the of data sample for calibration, n_v is the number of data sample for validation, $\hat{y}_i$ is the prediction value, y_i is measured value and y_m is mean value. The average differences between predicted and actual values were considered as bias (Eq. 4) and residual predictive deviation value (RPD) in Eq. 5.

$$Bias = \frac{1}{nv}\sum_{i=1}^{nv}(\hat{y}i - yi) \qquad \text{(Eq. 4)}$$

$$RPD = \frac{SD}{RMSEP} \qquad \text{(Eq. 5)}$$

2.4.2. Statistical Analysis.

All reference data (SSC and AA) were subjected to statistical analysis using R statistical software (version 4.0.4, R Core Team, Austria). Analysis of variance (ANOVA) was performed to determine significant differences in the physicochemical parameters between maturity stages and health conditions (normal vs. bronzed). Mean separations were conducted using Fisher's protected Least Significant Difference (LSD) test at a significance level of $p \leq 0.05$ (Abdullah *et al*., 2018; Magwaza *et al*., 2014).

3. RESULTS AND DISCUSSION

3.1 Distribution of Calibration and Prediction Reference Data

3.1.1 Rind Soluble Solids Concentration (SSC).

Rind soluble solids concentration (%SSC) varied significantly across maturity stages and between healthy and bronzed fruit (Tables 1 and 2). When averaged across health conditions, mean rind SSC increased from 3.68% at 10 weeks after anthesis (WAA) to 3.87% at 12 WAA, reaching 4.78% at 14 WAA. Interaction analysis (WAA × fruit condition) revealed significant effects ($p \leq 0.05$), indicating that maturation markedly influences rind sugar accumulation, particularly in healthy jackfruit (Figure 5).

At 14 WAA, healthy rind exhibited significantly higher SSC (5.44%) than bronzed rind (4.13%). Similarly, at 10 WAA, bronzed rind showed lower SSC (3.31%) compared to healthy rind (4.13%). This differential SSC profile suggests physiological disruptions associated with bronzing disease (*Pantoea stewartii* subsp. *stewartii*), potentially impairing normal carbohydrate accumulation in affected tissues (Abidin *et al.*, 2020; Ibrahim *et al.*, 2020). Abdullah *et al*., (2018) reported minimal SSC variation between rind segments, supporting our observation that SSC differences were primarily attributable to disease status rather than spatial tissue distribution.

The interaction between maturity stage (WAA) and health status (bronzed vs. healthy) significantly influenced rind SSC, revealing a consistent trend of increasing SSC with advancing maturity. This progressive accumulation of soluble solids aligns with established fruit developmental patterns, where sugars and other organic compounds typically increase as fruits near physiological maturity (Saxena *et al.*, 2015; Abdullah *et al*., 2018). Abdullah *et al.*, (2018) reported no significant SSC variation between rind sections, indicating biochemical uniformity within rind tissues. However, the observed differences between bronzed and healthy fruit confirm that disease states can disrupt carbohydrate accumulation, likely due to physiological impairments induced by *Pantoea stewartii* subsp. *stewartii* infection (Abidin *et al*., 2020; Ibrahim *et al.*, 2020).

As in other fruits, the increase in SSC during maturation is largely attributed to enhanced translocation of photosynthetic products, polysaccharide degradation, and reduced utilization of sugars as respiratory substrates during ripening (Nicolaï *et al*., 2007; Magwaza *et al*., 2014). The lower SSC in bronzed rinds likely reflects disruptions to these processes. These findings support earlier reports that rind tissues generally exhibit gradual soluble solids accumulation during

maturation; however, pathogen-induced stress, such as bronzing disease, can alter metabolic pathways, limit sugar accumulation, and ultimately diminish commercial fruit quality (Magwaza *et al.,* 2014; Nicolaï *et al.*, 2007).

3.1.2 Flesh Soluble Solids Concentration (SSC).

Flesh soluble solids concentration (SSC) exhibited a pronounced and consistent increase with advancing maturity, particularly in healthy fruit (Tables 1 and 3). Overall mean flesh SSC rose significantly from 4.38% at 10 WAA to 9.09% at 12 WAA, peaking at 10.01% at 14 WAA. Interaction effects (WAA × fruit condition) were highly significant ($p \leq 0.05$), revealing a marked divergence between healthy and bronzed fruit at later maturity stages (Figure 6).

In healthy fruit, flesh SSC increased sharply from 4.77% (10 WAA) to 13.43% (12 WAA), reaching 16.81% at 14 WAA. In contrast, bronzed flesh remained consistently low, with values of 4.07%, 4.85%, and 3.95% across the same stages. These trends align with Saxena *et al.* (2015), who reported significantly higher SSC in normal flesh than in rind or diseased tissues, due to enhanced sugar metabolism, organic acid degradation, and sugar accumulation during ripening. The higher SSC in healthy flesh reflects its role as the primary storage site for sugars, organic acids, minerals, and vitamins, whereas the decline in SSC in bronzed flesh after 12 WAA indicates disrupted biochemical maturation.

The persistently low SSC in bronzed flesh suggests severe metabolic impairment caused by *Pantoea stewartii* infection, which hinders sugar biosynthesis and accumulation (Zulperi *et al.*, 2017; Ibrahim *et al.,* 2020). As SSC is closely linked to sweetness, consumer acceptance, and market value, these findings confirm that bronzing disease severely compromises the internal quality and commercial potential of jackfruit (Magwaza *et al.*, 2014).

3.1.3 Flesh Ascorbic Acid (AA) Content.

Ascorbic acid (AA) content in jackfruit flesh varied markedly between healthy and bronzed fruit across maturity stages (Tables 4 and 5; Figure 7). In healthy fruit, AA decreased significantly from 25.31 mg/100 g FW (10 WAA) to 8.62 mg/100 g FW (14 WAA), consistent with typical ripening patterns as found in MD 2 pineapple (Ding and Syazwani, 2016). Bronzed flesh showed an atypical

trend, rising slightly from 13.75 mg/100 g FW (10 WAA) to 18.82 mg/100 g FW (12 WAA), before declining to 15.40 mg/100 g FW (14 WAA). This irregular pattern suggests pathogen-induced metabolic disruptions, with initial antioxidant upregulation followed by declines linked to tissue deterioration and resource depletion (Mijin *et al*., 2021; Lurie & Watkins, 2012; Hodges & Toivonen, 2008).

The significant interaction between maturity stage and health status underscores the complexity of biochemical responses under disease stress. In healthy fruit, AA decline reflects the typical inverse relationship with soluble solids accumulation, as organic acids are converted to sugars during ripening (Mijin, 2021; Ding & Syazwani, 2016). In bronzed fruit, *Pantoea stewartii* subsp. *stewartii* infection likely interferes with AA biosynthesis pathways, induces oxidative stress, and diverts metabolic resources towards defense, reducing antioxidant accumulation (Bhadwal & Sharma, 2010; Buthelezi, 2025; Zulperi *et al*., 2017; Mishra *et al.*, 2021).

These findings confirm that bronzing disease substantially diminishes jackfruit nutritional quality, potentially reducing consumer acceptance and market value. They also reinforce the value of rapid, non-destructive diagnostic tools such as Vis-NIRS for early disease detection and postharvest quality management, helping mitigate economic losses in commercial supply chains (Huang *et al*., 2025; Magwaza *et al.*, 2014).

3.1.4 Comparative Analysis between Rind and Flesh SSC Dynamics

Comparative analysis of rind and flesh tissues revealed clear physiological distinctions. Flesh consistently exhibited significantly higher SSC than rind, underscoring the metabolic specialization of fruit tissues during maturation (Saxena *et al*., 2015). In healthy fruit, flesh SSC increased progressively with maturity, reflecting its active role in carbohydrate accumulation, whereas rind SSC rose more slowly, consistent with its structural and protective functions (Abdullah *et al*., 2018).

Bronzing disease markedly altered expected ripening patterns in flesh at advanced maturity stages, with bronzed flesh showing stagnant or declining SSC. This suggests impaired carbohydrate accumulation and disrupted metabolic pathways (Zulperi *et al*., 2017), likely due to pathogen-

induced stress and defense responses diverting resources away from sugar storage and sweetness development (Pommerrenig *et al*., 2020).

These findings align with previous reports that pathogen stress can significantly disrupt fruit physiology, leading to deviations from normal ripening trajectories (Magwaza *et al*., 2014; Mishra *et al*., 2021). The ability of Vis-NIRS to detect such deviations in SSC profiles offers potential for early bronzing detection, enabling timely intervention and improved postharvest quality management in commercial jackfruit production.

The high predictive accuracy of Vis-NIRS chemometric models (Rv^2 = 0.94–0.97) demonstrates the feasibility and effectiveness of this approach as a rapid, non-destructive method for monitoring jackfruit quality attributes. Such predictive capability can greatly improve early detection of bronzing disease, enabling growers and stakeholders to implement targeted postharvest management strategies (Nicolaï *et al.*, 2007; Mishra *et al.*, 2021). These findings align with previous reports identifying Vis-NIRS as a powerful tool for quality assessment and disease prediction in various horticultural crops, supporting its broader adoption in commercial supply chains (Huang *et al*., 2025; Magwaza *et al*., 2014). To ensure reliable large-scale implementation, future research should validate these models under diverse environmental conditions, cultivars, and production seasons, thereby enhancing robustness and broadening applicability in commercial jackfruit operations.

3.2 Performance of Partial Least Squares Regression (PLSR) Calibration and Prediction Models Using Spectral Pretreatment Methods

In this study, Partial Least Squares Regression (PLSR) models were developed using spectral data between 500 and 950 nm (Figures 8 and 9). Seven spectral pretreatment methods—Multiplicative Scatter Correction (MSC), Standard Normal Variate (SNV), Moving Average, Gaussian Filter, Median Filter, Savitzky–Golay (SG) smoothing, and combinations of SG with SNV or MSC—were evaluated for their effectiveness in predicting soluble solids concentration (SSC) and ascorbic acid (AA) in *Artocarpus heterophyllus* cv. Tekam Yellow. For comparison, models using raw spectra without preprocessing were also assessed.

Model performance was evaluated using coefficients of determination for calibration (R^2c) and validation (R^2v) alongside root mean square errors for calibration (RMSEC) and validation (RMSEV), with high R^2 and low RMSE values indicating robust predictive accuracy (Nicolaï *et al*., 2007; Mishra *et al.*, 2021).

3.2.1 Chemometric Performance for SSC Prediction in Normal and Bronzing Rind Tissues Across Maturity Stages.

The calibration model for estimating soluble solids concentration (SSC) in normal rind at 10 weeks after anthesis (WAA) using 1,620 raw spectra demonstrated moderate predictive and calibration performance ($Rv^2 = 0.34$, RMSEV = 0.34% SSC; $Rc^2 = 0.36$, RMSEC = 0.78% SSC). Applying Savitzky–Golay smoothing (SG) combined with standard normal variate (SNV) preprocessing markedly enhanced performance, achieving Rv^2 and Rc^2 values of 0.97 each, with low RMSEV (0.38% SSC) and RMSEC (0.39% SSC) (Figure 10). This improvement is consistent with previous studies showing that scatter correction and smoothing filters can minimize baseline drifts and multiplicative scatter effects, thereby enhancing NIR predictive accuracy (Huang *et al*., 2025; Mishra *et al.*, 2021).

For bronzing rind SSC at 10 WAA, the raw spectral model similarly yielded moderate accuracy ($Rv^2 = 0.37$, RMSEV = 0.84% SSC; $Rc^2 = 0.36$, RMSEC = 0.86% SSC). SG + SNV preprocessing substantially improved robustness, producing $Rv^2 = 0.90$, RMSEV = 1.05% SSC, $Rc^2 = 0.91$, and RMSEC = 0.53% SSC (Figure 11), aligning with prior findings that SNV effectively reduces inter-sample variance and strengthens spectral calibration (Magwaza *et al*., 2014; Xia *et al*., 2020).

At 12 WAA, the raw model for normal rind SSC again showed moderate accuracy ($Rv^2 = 0.39$, RMSEV = 0.78% SSC; $Rc^2 = 0.35$, RMSEC = 0.84% SSC), which improved substantially after SG + SNV preprocessing ($Rv^2 = 0.93$, RMSEV = 0.68% SSC; $Rc^2 = 0.94$, RMSEC = 0.69% SSC) (Figure 12). Bronzing rind SSC at this stage followed the same pattern, with raw spectra performing moderately ($Rv^2 = 0.39$, RMSEV = 0.69% SSC; $Rc^2 = 0.39$, RMSEC = 0.72% SSC) and SG + SNV yielding robust results ($Rv^2 = 0.94$, RMSEV = 0.57% SSC; $Rc^2 = 0.94$, RMSEC = 0.57% SSC) (Figure 13). These improvements likely reflect compositional changes in rind tissues

with maturity, which pretreatment captures more precisely (Sánchez *et al*., 2012; Huang *et al*., 2025).

At 14 WAA, the raw model for normal rind SSC achieved moderate accuracy ($Rv^2 = 0.52$, RMSEV = 1.60% SSC; $Rc^2 = 0.53$, RMSEC = 1.56% SSC), while SG + SNV processing elevated performance to robust levels ($Rv^2 = 0.94$, RMSEV = 0.54% SSC; $Rc^2 = 0.94$, RMSEC = 0.52% SSC) (Figure 14). Bronzing rind SSC at this stage had the weakest raw model ($Rv^2 = 0.21$, RMSEV = 1.60% SSC; $Rc^2 = 0.20$, RMSEC = 1.65% SSC) but still benefited from preprocessing, improving to $Rv^2 = 0.83$, RMSEV = 0.74% SSC; $Rc^2 = 0.83$, RMSEC = 0.74% SSC (Figure 15).

Overall, the consistent performance gains achieved with SG + SNV preprocessing across all maturity stages and rind types underscore its value in reducing spectral noise and enhancing chemical signal detection. These findings corroborate previous reports on the efficacy of combining smoothing and scatter correction in developing accurate NIR calibration models for fruit quality assessment (Huang *et al*., 2025; Magwaza *et al*., 2014; Mishra *et al*., 2021; Xia *et al*., 2020; Wang *et al*., 2022).

3.2.2 Chemometric Performance for SSC Prediction in Normal and Bronzing Flesh Tissues Across Maturity Stages.

The calibration model for predicting soluble solids concentration (SSC) in normal flesh at 10 weeks after anthesis (WAA) using 810 raw spectra showed moderate calibration and validation accuracy, with $Rv^2 = 0.29$, RMSEV = 0.85% SSC, $Rc^2 = 0.29$, and RMSEC = 0.81% SSC. Applying Savitzky–Golay (SG) smoothing followed by standard normal variate (SNV) transformation substantially improved predictive capacity, yielding Rv^2=0.95, RMSEV = 1.31% SSC, $Rc^2 = 0.95$, and RMSEC = 1.34% SSC (Figure 16). This enhancement is consistent with findings in mango and pear, where SG + SNV preprocessing improved model robustness by reducing light scattering and noise artifacts (Rady & Guyer, 2015; Mishra *et al.*, 2021).

For bronzing flesh at 10 WAA, the raw spectral model also demonstrated moderate performance ($Rv^2 = 0.22$, RMSEV = 1.80% SSC, $Rc^2 = 0.22$, RMSEC = 1.12% SSC). With SG + SNV preprocessing, performance improved markedly ($Rv^2 = 0.94$, RMSEV = 1.26% SSC, $Rc^2 = 0.94$, RMSEC = 1.29% SSC), aligning with earlier reports on SNV's effectiveness in reducing

multiplicative scatter effects in Vis–NIR models in Figure 17 (Nicolaï *et al.*, 2007; Zhang *et al*., 2020).

At 12 WAA, the SSC model for normal flesh using raw spectra achieved $Rv^2 = 0.23$, RMSEV = 1.06% SSC, Rc^2 =0.19, and RMSEC = 1.34% SSC. SG + SNV pretreatment improved these values to $Rv^2 = 0.92$, RMSEV = 1.45% SSC, $Rc^2 = 0.92$, and RMSEC = 1.42% SSC (Figure 18). Similarly, for bronzing flesh, raw model performance was limited ($Rv^2 = 0.31$, RMSEV = 1.16% SSC, Rc^2 = 0.21, RMSEC = 1.20% SSC), but improved substantially after SG + SNV ($Rv^2 = 0.94$, RMSEV = 1.50% SSC, $Rc^2 = 0.94$, RMSEC = 1.50% SSC) (Figure 19).

At 14 WAA, the normal flesh SSC model from raw spectra yielded moderate accuracy ($Rv^2 = 0.57$, RMSEV = 2.28% SSC, Rc^2 = 0.58, RMSEC = 2.24% SSC). Post SG + SNV processing, performance improved ($Rv^2 = 0.75$, RMSEV = 1.72% SSC, $Rc^2 = 0.74$, RMSEC = 1.70% SSC), though still lower than at earlier stages (Figure 20). Similarly, for bronzing flesh, raw model performance was limited ($Rv^2 = 0.46$, RMSEV = 1.21% SSC, $Rc^2 = 0.45$, RMSEC = 1.21% SSC), but improved substantially after SG + MSC ($Rv^2 = 0.97$, RMSEV = 0.45% SSC, $Rc^2 = 0.97$, RMSEC = 1.71% SSC) (Figure 21). This decline may reflect physiological changes in tissue structure and composition during late maturation, affecting spectral absorption patterns, as also reported in other horticultural crops (Xia *et al*., 2020; Liu *et al*., 2022).

Overall, SG + SNV and SG + MSC preprocessing consistently enhanced model precision and generalizability by mitigating light scattering, path length variability, and instrument-induced distortions. The consistent gains across maturity stages confirm the chemometric robustness of Vis–NIR models when optimized with appropriate preprocessing, in agreement with previous fruit quality prediction research (Nicolaï *et al*., 2007; Zhang *et al*., 2020; Rady & Guyer, 2015).

3.2.3 Chemometric Performance for Ascorbic Acid (AA) Prediction in Normal and Bronzing Flesh Tissues Across Maturity Stages.

At 10 weeks after anthesis (WAA), the partial least squares regression (PLSR) model based on 810 raw spectra for predicting ascorbic acid (AA) concentration in normal flesh demonstrated moderate calibration and validation performance ($Rv^2 = 0.39$, RMSEV = 4.10 mg/100 g FW; Rc^2 = 0.41, RMSEC = 4.26 mg/100 g FW). Application of Savitzky–Golay (SG) smoothing combined

with multiplicative scatter correction (MSC) markedly improved predictive accuracy ($Rv^2 = Rc^2 = 0.99$; RMSEV = 1.33 mg/100 g FW; RMSEC = 1.34 mg/100 g FW) (Figure 22), confirming MSC's effectiveness in mitigating multiplicative light scatter caused by surface irregularities (Nicolaï *et al.*, 2007; Magwaza *et al.,* 2014). For bronzing flesh at 10 WAA, raw spectra yielded $Rv^2 = 0.37$, RMSEV = 3.80 mg/100 g FW, $Rc^2 = 0.35$, RMSEC = 3.98 mg/100 g FW, whereas SG + MSC preprocessing elevated performance to $Rv^2 = Rc^2 = 0.99$, RMSEV = 1.59 mg/100 g FW, and RMSEC = 1.58 mg/100 g FW (Figure 23).

At 12 WAA, the normal flesh model based on raw spectra exhibited weak predictive strength ($Rv^2 = Rc^2 = 0.26$; RMSEV = 4.74 mg/100 g FW; RMSEC = 4.81 mg/100 g FW). Implementation of SG + standard normal variate (SNV) preprocessing significantly enhanced accuracy ($Rv^2 = Rc^2 = 0.95$; RMSEV = RMSEC = 1.16 mg/100 g FW) (Figure 24). Similarly, bronzing flesh models improved from raw spectra values of $Rv^2 = 0.28$, RMSEV = 3.81 mg/100 g FW, $Rc^2 = 0.30$, RMSEC = 3.84 mg/100 g FW to SG + SNV values of $Rv^2 = Rc^2 = 0.95$, RMSEV = 1.32 mg/100 g FW, RMSEC = 1.33 mg/100 g FW (Figure 25), consistent with SNV's capacity to reduce pathlength and particle-size-related scatter (Mishra *et al*., 2021).

At 14 WAA, the raw spectra model for normal flesh had negligible predictive utility ($Rv^2 = Rc^2 = 0.06$; RMSEV = 2.44 mg/100 g FW; RMSEC = 2.36 mg/100 g FW), but SG + SNV preprocessing improved performance to $Rv^2 = 0.80$, RMSEV = 1.27 mg/100 g FW, $Rc^2 = 0.81$, RMSEC = 1.22 mg/100 g FW (Figure 26). For bronzing flesh, raw spectra yielded $Rv^2 = Rc^2 = 0.50$; RMSEV = 3.47 mg/100 g FW; RMSEC = 3.42 mg/100 g FW, while SG + SNV preprocessing enhanced these to $Rv^2 = Rc^2 = 0.96$; RMSEV = 0.72 mg/100 g FW; RMSEC = 0.71 mg/100 g FW (Figure 27).

Overall, SG + MSC (early stages) and SG + SNV (later stages) consistently improved model performance across maturity stages, in agreement with findings for citrus, apples, and pears where preprocessing effectively reduced non-chemical variability (Huang *et al*., 2025; Mishra *et al.*, 2021; Rady & Guyer, 2015; Magwaza *et al*., 2014). The stage-specific preprocessing choice underscores the importance of tailoring spectral correction strategies to tissue optical density and heterogeneity.

3.3 Evaluation of Partial Least Squares Regression (PLSR) Calibration and Prediction Models Using Spectral Pretreatments

Accurate prediction of internal fruit quality parameters using visible near-infrared spectroscopy (Vis-NIRS) is highly dependent on the spectral preprocessing methods applied before model construction. In this study, seven commonly used pretreatments—Multiplicative Scatter Correction (MSC), Standard Normal Variate (SNV), Moving Average, Gaussian Filter, Median Filter, Savitzky–Golay (SG), and combinations of SG with SNV or MSC—were evaluated. These techniques reduce spectral variability caused by fruit morphological differences, thereby improving model robustness and predictive accuracy (Nawi *et al*., 2013; Nicolaï *et al*., 2007). Spectral data (500–950 nm) from jackfruit rind and flesh were preprocessed using Unscrambler X software (version 10.3) before calibration and validation modeling.

3.3.1 Rind Soluble Solids Concentration (SSC) Prediction Performance.

The prediction performance of PLSR models for rind SSC varied substantially between raw and pretreated spectra. Consistent with earlier reports, pretreatment significantly enhanced model accuracy, underscoring its necessity for developing robust models (Mishra *et al*., 2021; Cen & He, 2007). For example, normal rind at 10 weeks after anthesis (WAA) exhibited moderate prediction accuracy without pretreatment (R^2p = 0.34, RMSEp = 0.34%), but improved markedly with SG+SNV preprocessing (R^2p = 0.97, RMSEp = 0.38%). A similar trend was observed for bronzed rind at 10 WAA, where prediction improved from moderate (R^2p = 0.37, RMSEp = 0.84%) to robust (R^2p = 0.90, RMSEp = 1.05%) following pretreatment.

The Residual Predictive Deviation (RPD) results further confirmed these improvements. As outlined by Saeys *et al.* (2005), RPD values above 2.5 indicate robust, reliable quantitative predictions. In this study, normal rind at 10 WAA achieved an RPD of 2.61 (Table 6), confirming excellent predictive performance. Even models with moderate RPD values (1.5–2.5)—such as bronzed rind at 12 WAA (RPD = 1.61)—were considered suitable for approximate quantitative predictions, aligning with the criteria suggested by Davey *et al*. (2009) and Magwaza *et al*. (2014).

3.3.2 Flesh Soluble Solids Concentration (SSC) Prediction Performance.

Compared with rind models, flesh SSC predictions demonstrated lower accuracy, reflecting the greater variability and biochemical complexity of flesh tissues (Saxena *et al.*, 2015; Nicolaï *et al*., 2007). For example, flesh SSC models for normal jackfruit at 10 WAA achieved only moderate

predictive performance even after pretreatment (R^2p = 0.95, RMSEp = 1.31%), corresponding to a low RPD value (0.72) (Table 7). Such reduced performance in flesh tissues is consistent with previous studies (Cozzolino *et al*., 2011; Magwaza *et al.*, 2014), which attributed it to biochemical heterogeneity and variable moisture content, both of which can compromise spectral consistency.

Interestingly, bronzed flesh tissues at advanced maturity (e.g., 14 WAA) yielded high R^2 values (0.97) but also exhibited relatively large RMSEp (1.67%), suggesting that disease-induced biochemical changes may complicate prediction accuracy. This finding supports earlier reports (Wang *et al*., 1991; Magwaza *et al*., 2014) indicating that external factors—such as orchard location and pathogen presence—can destabilize models, increase bias, and contribute to greater prediction variability (Table 7).

3.3.3 Flesh Ascorbic Acid (AA) Content Prediction Performance.

The flesh AA models displayed variable prediction performance depending on maturity stage and health status (Table 8). For normal flesh at 10 WAA, spectral pretreatment yielded outstanding accuracy (R^2p = 0.99, RMSEp = 1.33 mg/100 g FW), with an acceptable level of predictive reliability (RPD = 0.75, Table 6). In contrast, bronzed flesh showed lower predictive stability, likely due to pathogen-induced stress and associated biochemical pathway alterations, as reported by Zulperi *et al*. (2017) and Lurie & Watkins (2012).

By 14 WAA, predictive accuracy for normal flesh decreased markedly (R^2p = 0.80), reflecting heightened biochemical variability as fruit neared full maturity (Lee & Kader, 2000). Interestingly, bronzed flesh at the same stage exhibited unexpectedly strong performance (R^2p = 0.96, RMSEp = 0.72 mg/100 g FW, RPD = 1.33). This improvement may be attributed to pathogen-specific spectral features that enhance chemometric discrimination in infected tissues (Cozzolino *et al*., 2011; Mishra *et al*., 2021).

3.3.4 Model Robustness, Limitations, and Recommendations.

While spectral pretreatment substantially improved prediction accuracy and robustness, the variability observed in flesh predictions—particularly under disease conditions—highlights inherent limitations of chemometric models derived from single-orchard spectral datasets.

Magwaza *et al*. (2014) likewise cautioned against overgeneralizing calibration models built from restricted datasets, noting that external factors such as geographic variation and environmental conditions can markedly influence predictive reliability.

In our study, higher bias values were evident, especially for flesh SSC at advanced maturity (e.g., 14 WAA), suggesting instability arising from discrepancies between calibration and validation sets. This finding reflects a violation of the fundamental principle outlined by Wang *et al*. (1991), who stressed the importance of incorporating representative variability within calibration data.

To strengthen future model robustness, we recommend expanding calibration datasets to include spectral measurements from multiple orchards, harvest cycles, and diverse growing environments. Such an approach would help mitigate prediction bias and enhance generalizability, thereby supporting the broader commercial adoption of non-destructive spectroscopy for fruit quality assessment (Cozzolino *et al.*, 2011; Nicolaï *et al*., 2007; Mishra *et al*., 2021).

4. CONCLUSION

This study demonstrated the potential of visible–near-infrared spectroscopy (Vis-NIRS) as a non-invasive method for assessing internal fruit quality across ripening stages and under disease pressure. Optimized spectral preprocessing, particularly Savitzky–Golay smoothing combined with scatter correction (SNV, MSC), significantly improved predictive accuracy for soluble solids concentration and ascorbic acid content. Distinct spectral signatures linked to bronzing provide a basis for early detection and informed postharvest management.

Rind-based models showed strong predictive performance and practical utility, although mature flesh predictions were less consistent due to metabolic complexity and disease-induced variability. Expanding calibration datasets to encompass diverse orchards, environments, and harvest cycles is essential for enhancing model robustness and generalizability.

Safeguarding the industry against bronzing requires an integrated strategy that combines advanced diagnostic tools, sustained research, effective grower engagement, and supportive policy measures. Vis-NIRS, when embedded within such a framework, offers a scalable pathway toward a more resilient and economically viable jackfruit sector.

However, limitations remain, particularly regarding the prediction consistency in mature flesh tissues where metabolic complexity increases and disease-induced variability becomes more pronounced. These findings underscore the importance of enriching the dataset with broader agro-ecological representations, including samples from diverse geographic zones, orchard conditions, and seasonal cycles. Expanding the training dataset would enhance model robustness and generalizability, minimizing prediction bias and facilitating commercial scalability.

In conclusion, ensuring the resilience of the jackfruit industry against bronzing disease necessitates a holistic and integrated approach. This includes sustained scientific inquiry, the adoption of smart agricultural technologies, strengthened extension services, and supportive policy frameworks. By fostering synergy among researchers, growers, and decision-makers, Malaysia can harness innovative tools like Vis-NIRS to build a more sustainable, disease-resilient, and economically vibrant jackfruit sector.

Acknowledgements

The authors gratefully acknowledge the facilities and technical support provided by the Department of Crop Science, Faculty of Agriculture; the Department of Biological and Agricultural Engineering, Faculty of Engineering; and the Institute of Plantation Studies, Universiti Putra Malaysia.

REFERENCES

Abdullah, N., Nawi, N. M., Ding, P., Kassim, M. S. M., & Lazim, S.S.R.M. (2018). Preliminary study to predict moisture content of jackfruit skin using shortwave near infrared spectroscopy. https://doi.org/10.26656/fr.2017.3(2).135

Abidin, N., Ismail, S. I., Vadamalai, G., Yusof, M. T., Hakiman, M., Karam, D. S., Ismail-Suhaimy, N. W., Ibrahim, R., & Zulperi, D. (2020). Genetic diversity of *Pantoea stewartii* subspecies *stewartii* causing jackfruit-bronzing disease in Malaysia. *PLOS ONE*, *15*(6), e0234350. https://doi.org/10.1371/journal.pone.0234350

Ali, M. M., Hashim, N., & Shahamshah, M. I. (2021). Durian (*Durio zibethinus*) ripeness detection using thermal imaging with multivariate analysis. *Postharvest Biology and Technology*, *176*, 111517. https://doi.org/10.1016/j.postharvbio.2021.111517

Azad, A. K., Jones, J. G., & Haq, N. (2007). Assessing morphological and isozyme variation of jackfruit (*Artocarpus heterophyllus* Lam.) in Bangladesh. *Agroforestry Systems*, *71*(2), 109–125. https://doi.org/10.1007/s10457-007-9039-8

Bobelyn, E., Serban, A. S., Nicu, M., Lammertyn, J., Nicolai, B. M., & Saeys, W. (2010). Postharvest quality of apple predicted by NIR-spectroscopy: Study of the effect of biological variability on spectra and model performance. *Postharvest Biology and Technology*, *55*(3), 133–143. https://doi.org/10.1016/j.postharvbio.2009.09.006

Bhadwal, J., & Sharma, Y. P. (2010). Changes in ascorbic acid content of fresh apricot fruits under fungal pathogenesis. *Environment Conservation Journal*, *11*(3), 33-36. https://doi.org/10.36953/ECJ.2010.110307

Bui, T. T., Wright, S. A., Falk, A. B., Vanwalleghem, T., Van Hemelrijck, W., Hertog, M. L., ... & Davey, M. W. (2019). Botrytis cinerea differentially induces postharvest antioxidant responses in 'Braeburn' and 'Golden Delicious' apple fruit. *Journal of the Science of Food and Agriculture*, *99*(13), 5662-5670. https://doi.org/10.1002/jsfa.9827

Buthelezi, N. M. D. (2025). Chitosan–Zinc Oxide Nanoparticle Composite Coatings Preserve Postharvest Quality of 'Rosada' Cherry Tomato. *HortScience*, *60*(4), 613-623. https://doi.org/10.21273/HORTSCI18426-24

Cen, H., & He, Y. (2007). Theory and application of near infrared reflectance spectroscopy in determination of food quality. *Trends in Food Science & Technology*, *18*(2), 72–83. https://doi.org/10.1016/j.tifs.2006.09.003

Chakraborty, A., Panda, J., Mishra, A. K., Sivakumar, S., Srinivasan, L. V., Nongbet, A., ... & Mohanta, Y. K. (2025). Jackfruit waste for the production of sustainable biorefinery products: a step towards bio-economic advancement. *Biomass Conversion and Biorefinery*, *15*(7), 9801-9823. https://doi.org/10.1007/s13399-024-05954-y

Clark, C. J., McGlone, V. A., De Sil va, H. N., Manning, M. A., Burdon, J., & Mowat, A. D. (2004). Prediction of storage disorders of kiwifruit (*Actinidia chinensis*) based on visible-NIR spectral characteristics at harvest. *Postharvest Biology and Technology*, *32*(2), 147–158. https://doi.org/10.1016/j.postharvbio.2003.11.004

Cozzolino, D., Cynkar, W. U., Shah, N., & Smith, P. (2011). Multivariate data analysis applied to spectroscopy: Potential application to juice and fruit quality. *Food Research International*, *44*(7), 1888–1896. https://doi.org/10.1016/j.foodres.2011.01.041

Davey, M. W., Saeys, W., Hof, E., Ramon, H., Swennen, R. L., & Keulemans, J. (2009). Application of Visible and Near-Infrared Reflectance Spectroscopy (Vis/NIRS) to Determine Carotenoid Contents in Banana (*Musa spp*.) Fruit Pulp. *Journal of Agricultural and Food Chemistry*, *57*(5), 1742–1751. https://doi.org/10.1021/jf803137d

Ding, P., & Syazwani, S. (2016). Physicochemical quality, antioxidant compounds and activity of MD-2 pineapple fruit at five ripening stages. *International Food Research Journal, 23*(2), 549–555. http://www.ifrj.upm.edu.my

Fraser, D. G., Jordan, R. B., Künnemeyer, R., & McGlone, V. A. (2003). Light distribution inside mandarin fruit during internal quality assessment by NIR spectroscopy. *Postharvest Biology and Technology*, *27*(2). https://doi.org/10.1016/S0925-5214(02)00058-3

Gapasin, R. M., Garcia, R. P., Advincula, C. T., De la Cruz, C. S., & Borines, L. M. (2014). Fruit Bronzing, a New Disease Affecting Jackfruit Caused by (Smith) Mergaert *Pantoea stewartii et al*. *Annals of Tropical Research*, 17–31. https://doi.org/10.32945/atr3612.2014

Hernández-Morales, A., Pérez-Casillas, J. M., Soria-Guerra, R. E., Velázquez-Fernández, J. B., & Arvizu-Gómez, J. L. (2017). First report of *Pantoea stewartii* subsp. *stewartii* causing jackfruit bronzing disease in Mexico. *Journal of Plant Pathology*, *99*(3), 807. http://www.sipav.org/main/jpp/index.php/jpp/article/view/3969/2613

Hernández-Morales, A., Soria-Guerra, R.E., & Isiordia-Aquino, N. *et al.* (2021). Association of *Pantoea stewartii* subsp. *stewartii* with ChrysSA genus flea beetles in jackfruit crops. *Journal of Plant Pathology*, 103**,** 539–547. https://doi.org/10.1007/s42161-021-00787-4

Hodges, D. M., & Toivonen, P. M. (2008). Quality of fresh-cut fruits and vegetables as affected by exposure to abiotic stress. *Postharvest Biology and Technology*, *48*(2), 155-162. https://doi.org/10.1016/j.postharvbio.2007.10.016

Huang, Y., Zheng, Y., Liu, P., Xie, L., & Ying, Y. (2025). Enhanced prediction of soluble solids content and vitamin C content in citrus using visible and near-infrared spectroscopy combined with one-dimensional convolutional neural network. *Journal of Food Composition and Analysis*, *139*, 107131. https://doi.org/10.1016/j.jfca.2024.107131

Ibrahim, R., Ismail-Suhaimy, N. W., Shu-Qing, T., Ismail, S. I., Abidin, N., Hakiman, M., Karam, D. S., Ahmad-Hamdani, M. S., Yusof, M. T., & Zulperi, D. (2020). Molecular characterization and phylogenetic analysis of *Pantoea stewartii* subspecies *stewartii* causing bronzing disease of jackfruit in Malaysia based on *cps* and *hrp* gene sequences. *Journal of Plant Pathology*, *102*(1), 193–199. https://doi.org/10.1007/s42161-019-00383-7

Lammertyn, J., Peirs, A., De Baerdemaeker, J., & Nicolaï, B. (2000). Light penetration properties of NIR radiation in fruit with respect to non-destructive quality assessment. *Postharvest Biology and Technology*, *18*(2). https://doi.org/10.1016/S0925-5214(99)00071-X

Lee, S. K., & Kader, A. A. (2000). Preharvest and postharvest factors influencing vitamin C content of horticultural crops. *Postharvest biology and technology*, *20*(3), 207-220 https://doi.org/10.1016/S0925-5214(00)00133-2

Liu, D., Wang, E., Wang, G., & Ma, G. (2022). Nondestructive determination of soluble solids content, firmness, and moisture content of “Longxiang” pears during maturation using near-infrared spectroscopy. *Journal of Food Processing and Preservation*, *46*(3), e16332. https://doi.org/10.1111/jfpp.16332

Lurie, S., & Watkins, C. B. (2012). Superficial scald, its etiology and control. *Postharvest biology and Technology*, *65*, 44-60. https://doi.org/10.1016/j.postharvbio.2011.11.001

Magwaza, L. S., Opara, U. L., Cronje, P. J. R., Landahl, S., Nieuwoudt, H. H., Mouazen, A. M., Nicolaï, B. M., & Terry, L. A. (2014). Assessment of rind quality of 'Nules Clementine' mandarin fruit during postharvest storage: 2. Robust Vis/NIRS PLS models for prediction of physico-chemical attributes. *Scientia Horticulturae*, *165*, 421–432. https://doi.org/10.1016/j.scienta.2013.09.050

Mijin, S., Ding, P., Saari, N., & Ramlee, S. I. (2021). Effects of pollination techniques and harvesting stage on the physico-chemical characteristics of jackfruit. *Scientia Horticulturae*, *285*, 110199. https://doi.org/10.1016/j.scienta.2021.110199

Mishra, P., Woltering, E., Brouwer, B., & Hogeveen-van Echtelt, E. (2021). Improving moisture and soluble solids content prediction in pear fruit using near-infrared spectroscopy with variable selection and model updating approach. *Postharvest Biology and Technology*, *171*, 111348. https://doi.org/10.1016/j.postharvbio.2020.111348

Nawi, N. M., Chen, G., Jensen, T., & Mehdizadeh, S. A. (2013). Prediction and classification of sugar content of sugarcane based on skin scanning using visible and shortwave near infrared. *Biosystems Engineering*, *115*(2), 154-161. https://doi.org/10.1016/j.biosystemseng.2013.03.005

Nicolaï, B. M., Beullens, K., Bobelyn, E., Peirs, A., Saeys, W., Theron, K. I., & Lammertyn, J. (2007). Nondestructive measurement of fruit and vegetable quality by means of NIR spectroscopy: A review. *Postharvest Biology and Technology*, *46*(2), 99–118. https://doi.org/10.1016/j.postharvbio.2007.06.024

Nielsen, S. S. (2024). Vitamin C determination by indophenol method. In *Nielsen's food analysis laboratory manual* (pp. 153-156). Cham: Springer International Publishing. https://doi.org/10.1007/978-3-031-44970-3_18

Pommerrenig, B., Müdsam, C., Kischka, D., & Neuhaus, H. E. (2020). Treat and trick: common regulation and manipulation of sugar transporters during sink establishment by the plant and the pathogen. *Journal of Experimental Botany*, *71*(14), 3930-3940. Available: https://doi.org/10.1093/jxb/eraa168

Rady, A. M., & Guyer, D. E. (2015). Evaluation of sugar content in potatoes using NIR reflectance and wavelength selection techniques. *Postharvest Biology and Technology*, *103*, 17-26. https://doi.org/10.1016/j.postharvbio.2015.02.012

Rungpichayapichet, P., Mahayothee, B., Nagle, M., Khuwijitjaru, P., & Müller, J. (2016). Robust NIRS models for non-destructive prediction of postharvest fruit ripeness and quality in mango. Postharvest Biology and Technology, 111, 31–40. https://doi.org/10.1016/j.postharvbio.2015.07.006

Saeys, W., Mouazen, A. M., & Ramon, H. (2005). Potential for onsite and online analysis of pig manure using visible and near infrared reflectance spectroscopy. *Biosystems Engineering*, 91(4), 393-402. https://doi.org/10.1016/j.biosystemseng.2005.05.001

Sánchez, N. H., Lurol, S., Roger, J. M., & Bellon-Maurel, V. (2003). Robustness of models based on NIR spectra for sugar content prediction in apples. *Journal of Near Infrared Spectroscopy*, *11*(2), 97-107. https://opg.optica.org/jnirs/abstract.cfm?URI=jnirs-11-2-97

Saxena, A., Bawa, A. S., & Raju, P. S. (2011). Jackfruit (*Artocarpus heterophyllus* Lam.). In *Postharvest Biology and Technology of Tropical and Subtropical Fruits* (pp. 275–299e). Elsevier. https://doi.org/10.1533/9780857092885.275

Saxena, A., Maity, T., Raju, P. S., & Bawa, A. S. (2015). Optimization of pretreatment and evaluation of quality of jackfruit (*Artocarpus heterophyllus*) bulb crisps developed using combination drying. *Food and Bioproducts Processing*, *95*, 106–117. https://doi.org/10.1016/j.fbp.2015.04.005

Voon, Y. Y., Hamid, N. S. A., Rusul, G., Osman, A., & Quek, S. Y. (2006). Physicochemical, microbial and sensory changes of minimally processed durian (*Durio zibethinus* cv. D24) during storage at 4 and 28°C. *Postharvest Biology and Technology*, *42*(2), 168–175. https://doi.org/10.1016/j.postharvbio.2006.06.006

Wang, H. P., Chen, P., Dai, J. W., Liu, D., Li, J. Y., Xu, Y. P., & Chu, X. L. (2022). Recent advances of chemometric calibration methods in modern spectroscopy: Algorithms, strategy, and related issues. *TrAC Trends in Analytical Chemistry*, *153*, 116648. https://doi.org/10.1016/j.trac.2022.116648

Wang, Yongdong., Veltkamp, D. J., & Kowalski, B. R. (1991). Multivariate instrument standardization. *Analytical Chemistry*, *63*(23), 2750–2756. https://doi.org/10.1021/ac00023a016

Xia, Y., Fan, S., Li, J., Tian, X., Huang, W., & Chen, L. (2020). Optimization and comparison of models for prediction of soluble solids content in apple by online Vis/NIR transmission coupled with diameter correction method. *Chemometrics and Intelligent Laboratory Systems*, *201*, 104017. https://doi.org/10.1016/j.chemolab.2020.104017

Zhang, W., Wang, A., Lv, Z., & Gao, Z. (2020). Nondestructive measurement of kiwifruit firmness, soluble solid content (SSC), titratable acidity (TA), and sensory quality by vibration spectrum. *Food science & nutrition*, *8*(2), 1058-1066. https://doi.org/10.1002/fsn3.1390

Zulperi, D., Manaf, N., Ismail, S. I., Karam, D. S., & Yusof, M. T. (2017). First Report of *Pantoea stewartii* subsp. *stewartii* Causing Fruit Bronzing of Jackfruit (*Artocarpus heterophyllus*), a New Emerging Disease in Peninsular Malaysia. *Plant Disease*, *101*(5), 831–831. https://doi.org/10.1094/PDIS-11-16-1689-PDN

Conflict of Interest: The authors declare that the research was conducted in the absence of any commercial or financial relationship that could be construed as a potential conflict of interest.

TABLES

Table 1: Main and interaction effects of week after anthesis and fruit condition on the rind and flesh soluble solids concentration of jackfruit cv. Tekam Yellow.

Factor	Rind Soluble Solids Concentration (%SSC)	Flesh Soluble Solids Concentration (%SSC)
Weeks after anthesis (WAA)		
10	3.68b[x]	4.38c
12	3.87b	9.09b
14	4.78a	10.01a
Fruit Condition (H)		
Normal (N)	4.37a	11.71a
Bronzing (B)	3.87b	4.27b
Interaction		
WAA x H	***	***

[x] For each factor, mean comparisons within the factors followed by the different letters are significantly different by LSD at $p \leq 0.05$. ***, highest significant at $p \leq 0.001$, respectively

Table 2: Mean and standard deviation for rind soluble solids concentration of fruit condition in maturity stages.

Fruit Condition	Weeks	Mean	SD	Interaction of Fruit Condition within Weeks	Pretreatment
Normal	10	4.13b	0.99	***	SG + SNV
Bronzing	10	3.31c	1.08	***	SG + SNV
Normal	12	3.52c	1.05	***	SG + SNV
Bronzing	12	4.22b	0.92	***	SG + SNV
Normal	14	5.44a	2.30	***	SG + SNV
Bronzing	14	4.13b	1.87	***	SG + SNV

Table 3: Mean and standard deviation for flesh soluble solids concentration of fruit condition in maturity stages.

Fruit Condition	Weeks	Mean	SD	Interaction of Fruit Condition within Weeks	Pretreatment
Normal	10	4.77c	0.98	***	SG + SNV
Bronzing	10	4.07d	1.28	***	SG + SNV
Normal	12	13.43b	1.52	***	SG + SNV
Bronzing	12	4.85c	1.41	***	SG + SNV
Normal	14	16.81a	3.46	***	SG + SNV
Bronzing	14	3.95d	1.65	***	SG + MSC

Table 4: Main and interaction effects of week after anthesis and fruit condition condition on the flesh ascorbic acid of jackfruit cv. Tekam Yellow.

Factor	**Flesh Ascorbic Acid (mg / 100 g FW)**
Weeks after anthesis (WAA)	
10	18.98b[x]
12	19.95a
14	12.24c
Fruit Condition (H)	
Normal (N)	18.39a
Bronzing (B)	15.85b
Interaction	
WAA x H	***

[x] For each factor, mean comparisons within the factors followed by the different letters are significantly different by LSD at $p \leq 0.05$. ***, highest significant at $p \leq 0.001$, respectively.

Table 5: Mean and standard deviation for flesh ascorbic acid of fruit condition in maturity stages.

Fruit Condition	Weeks	Mean	SD	Interaction of Fruit Condition within Weeks	Pretreatment
Normal	10	25.31a	5.62	***	SG + MSC
Bronzing	10	13.75e	5.59	***	SG + MSC
Normal	12	21.09b	5.65	***	SG + SNV
Bronzing	12	18.82c	4.64	***	SG + SNV
Normal	14	8.62f	2.45	***	SG + SNV
Bronzing	14	15.40d	4.86	***	SG + SNV

Table 6: Preformation of PLSR Calibration and Prediction Model in Predicting Rind Soluble Solids Concentration of Maturity Stages

Fruit Condition	Weeks	LVs	Rc^2	RMSEc	Rp^2	RMSEp	Bias	Slope	Offset	Correlation	RPD
Normal	10	7	0.97	0.39	0.97	0.38	-0.02	0.97	0.19	0.98	2.61
Bronzing	10	7	0.91	0.53	0.90	0.53	0.01	0.91	0.61	0.95	2.04
Normal	12	7	0.94	0.69	0.93	0.68	0.04	0.92	0.41	0.97	1.54
Bronzing	12	5	0.94	0.57	0.94	0.57	0.00	0.95	0.30	0.97	1.61
Normal	14	7	0.94	0.52	0.94	0.54	-0.01	0.95	0.31	0.97	4.26
Bronzing	14	7	0.83	0.74	0.83	0.74	0.00	0.84	0.96	0.91	2.53

Table 7: Preformation of PLSR Calibration and Prediction Model in Predicting Flesh Soluble Solids Concentration of Maturity Stages.

Fruit Condition	Weeks	LVs	Rc^2	RMSEc	Rp^2	RMSEp	Bias	Slope	Offset	Correlation	RPD
Normal	10	7	0.95	1.34	0.95	1.31	0.02	0.95	0.67	0.97	0.72
Bronzing	10	7	0.94	1.29	0.94	1.26	0.08	0.94	0.65	0.97	0.74
Normal	12	7	0.92	1.42	0.92	1.45	-0.05	0.93	0.46	0.96	0.63
Bronzing	12	7	0.94	1.56	0.94	1.50	0.00	0.94	0.51	0.97	0.63
Normal	14	7	0.74	1.70	0.75	1.72	-0.04	0.74	1.12	0.87	0.43
Bronzing	14	7	0.97	1.71	0.97	1.67	0.84	0.98	0.40	0.99	0.58

Table 8: Preformation of PLSR Calibration and Prediction Model in Predicting Flesh Ascorbic acid of Maturity Stages.

Fruit Condition	Weeks	LVs	Rc^2	RMSEc	Rp^2	RMSEp	Bias	Slope	Offset	Correlation	RPD
Normal	10	2	0.99	1.34	0.99	1.33	-0.02	0.99	0.28	0.99	0.75
Bronzing	10	3	0.99	1.59	0.99	1.59	0.00	0.99	0.01	0.99	0.62
Normal	12	7	0.95	1.17	0.95	1.16	-0.02	0.95	0.40	0.98	0.82
Bronzing	12	5	0.95	1.33	0.95	1.32	-0.03	0.95	0.44	0.98	0.72
Normal	14	7	0.81	1.22	0.80	1.27	-0.01	0.81	0.62	0.90	0.64
Bronzing	14	7	0.96	0.71	0.96	0.72	-0.01	0.97	0.12	0.98	1.33

FIGURES

Figure 1: Divided 30 portions from top to bottom

Figure 2: Experimental set up for spectrometer

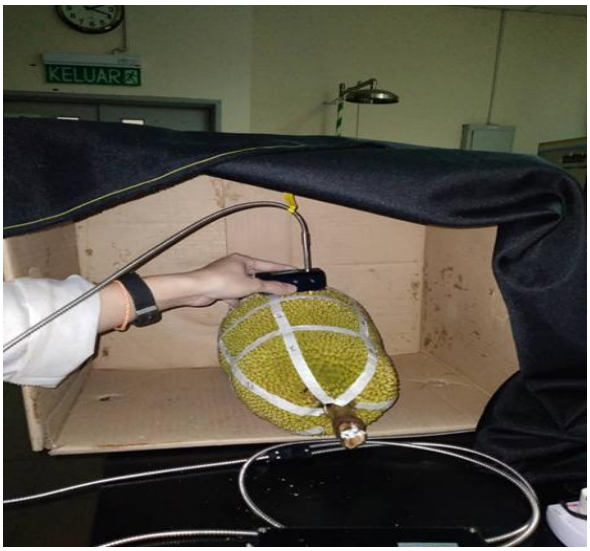

Figure 3: Radiation penetrated on the rind on each portion using spectrometer

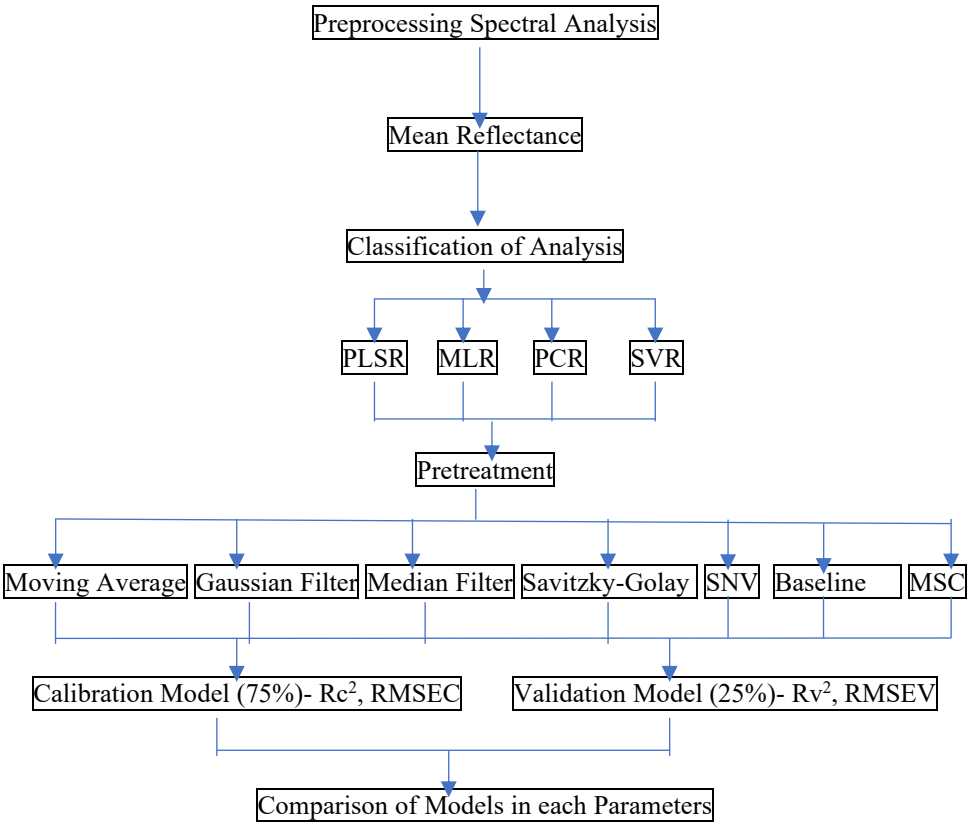

Figure 4: Flowchart of image preprocessing and data analysis for predicting apple fruit quality

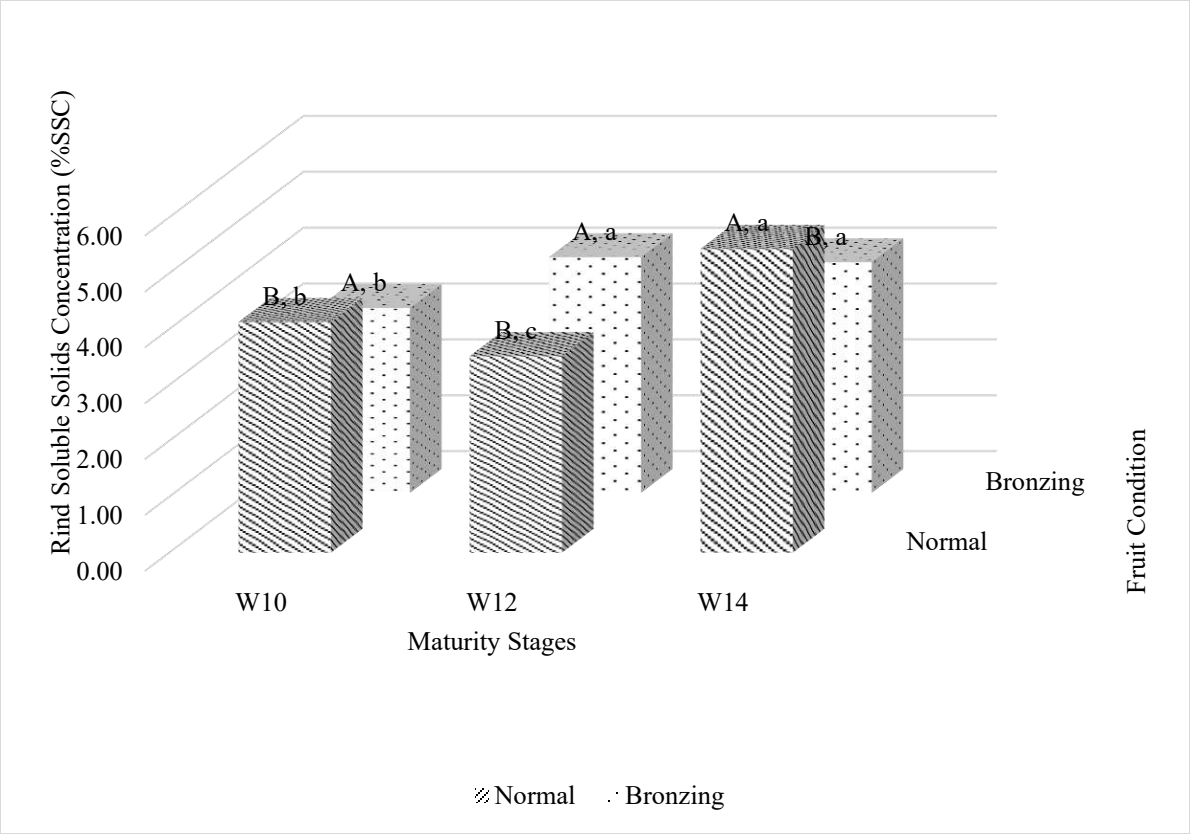

Figure 5: Effects of fruit condition and maturity stages (weeks after anthesis) on rind soluble solids concentration of jackfruit cv. Tekam Yellow. Means separation followed by different capital and small letters are significantly different ($p \leq 0.05$) using LSD between fruit condition and maturity stages (weeks after anthesis), respectively.

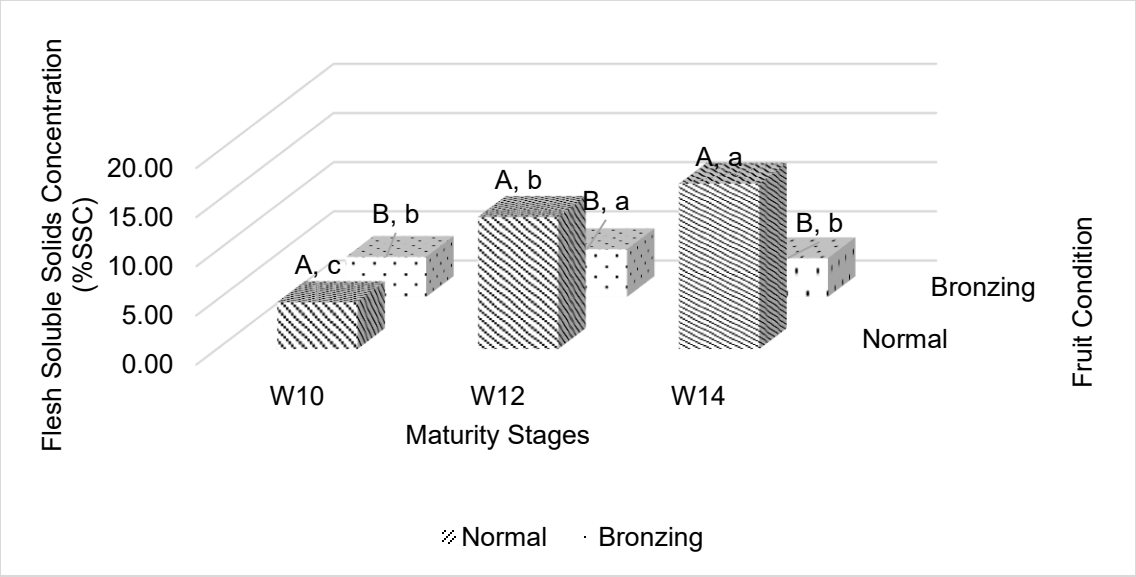

Figure 6: Effects of fruit condition and maturity stages (weeks after anthesis) on flesh soluble solids concentration of jackfruit cv. Tekam Yellow. Means separation followed by different capital and small letters are significantly different ($p \leq 0.05$) using LSD between fruit condition and maturity stages (weeks after anthesis), respectively.

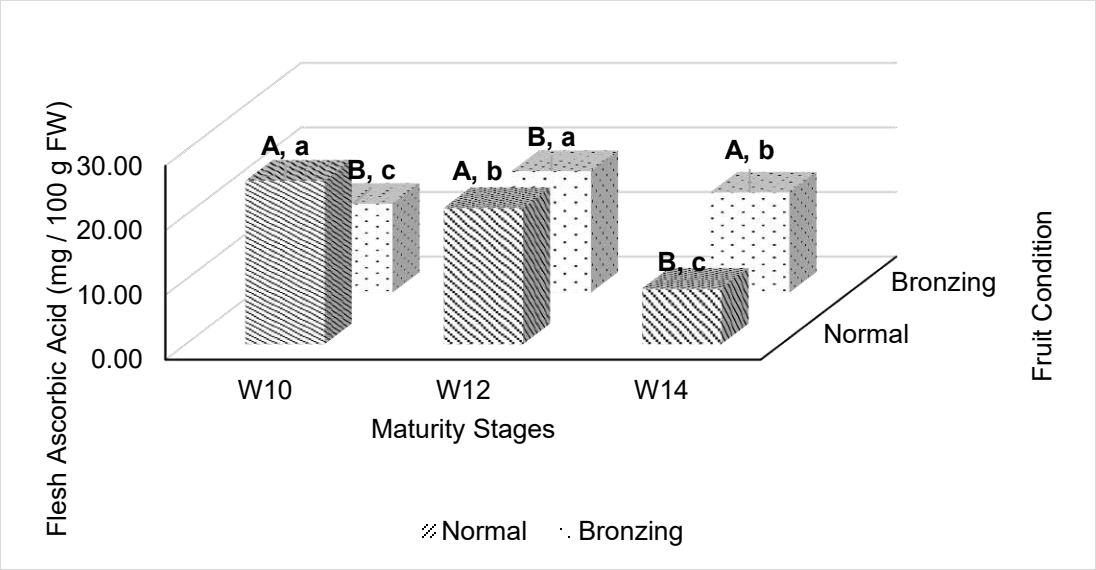

Figure 7: Effects of fruit condition and maturity stages (weeks after anthesis) on flesh ascorbic acid of jackfruit cv. Tekam Yellow. Means separation followed by different capital and small letters are significantly different ($p \leq 0.05$) using LSD between fruit condition and maturity stages (weeks after anthesis), respectively.

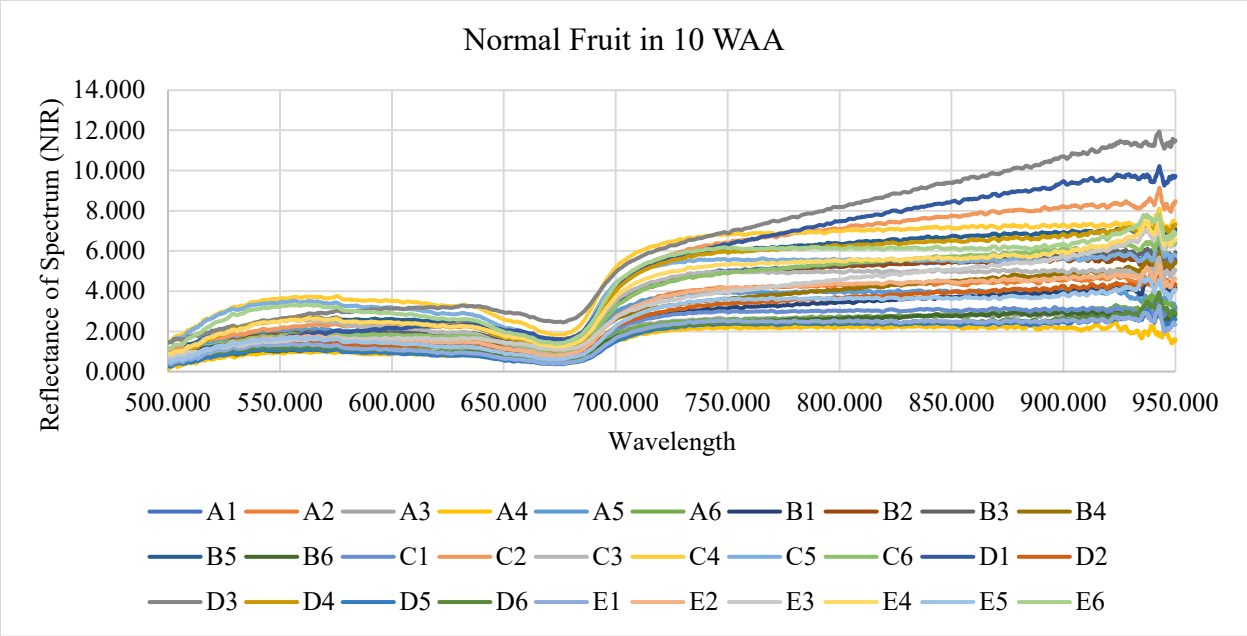

*The rind was systematically segmented into five layers—top (A1 to A6), middle-top (B1 to B6), middle (C1 to C6), middle-bottom (D1 to D6), and bottom (E1 to E6)—to assess spatial spectral variability.
Figure 8: Typical NIR reflectance spectrum of normal fruit in 10 WAA

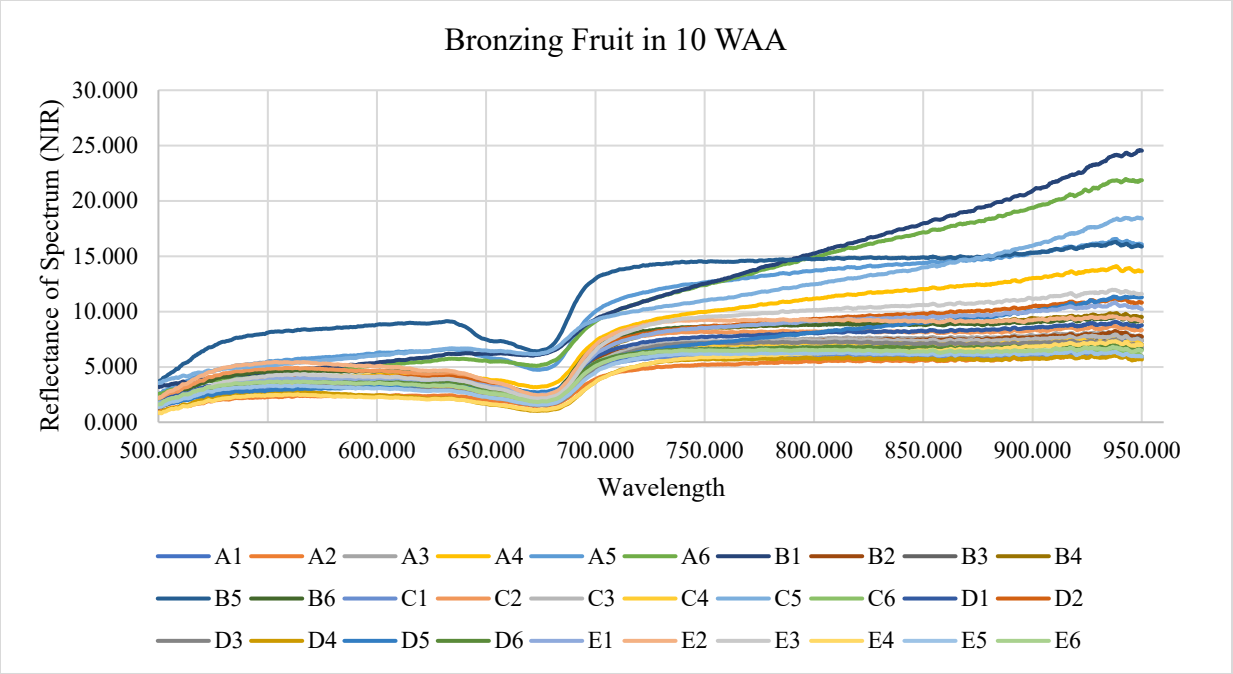

*The rind was systematically segmented into five layers—top (A1 to A6), middle-top (B1 to B6), middle (C1 to C6), middle-bottom (D1 to D6), and bottom (E1 to E6)—to assess spatial spectral variability.
Figure 9: Typical NIR reflectance spectrum of bronzing fruit in 10 WAA

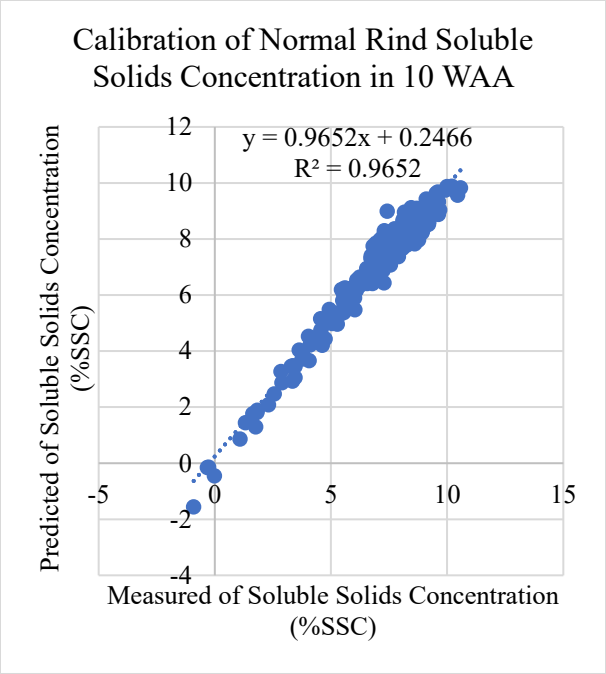

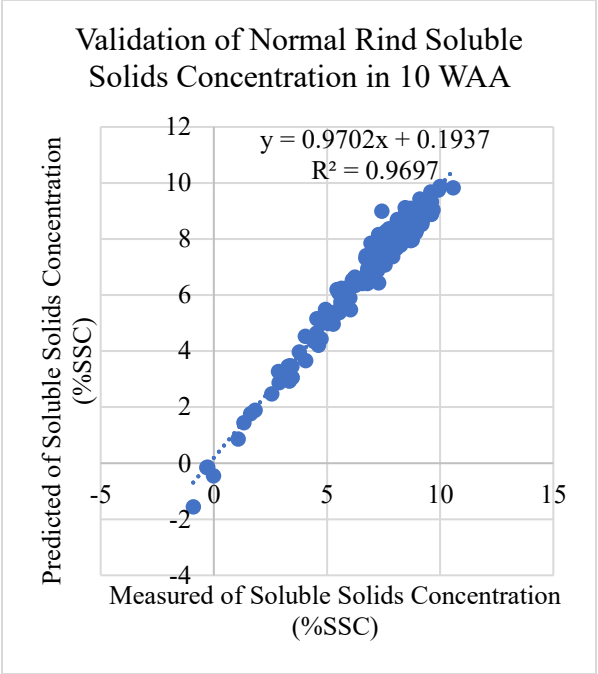

Figure 10: Calibration and validation of normal rind soluble solids concentration in 10 WAA

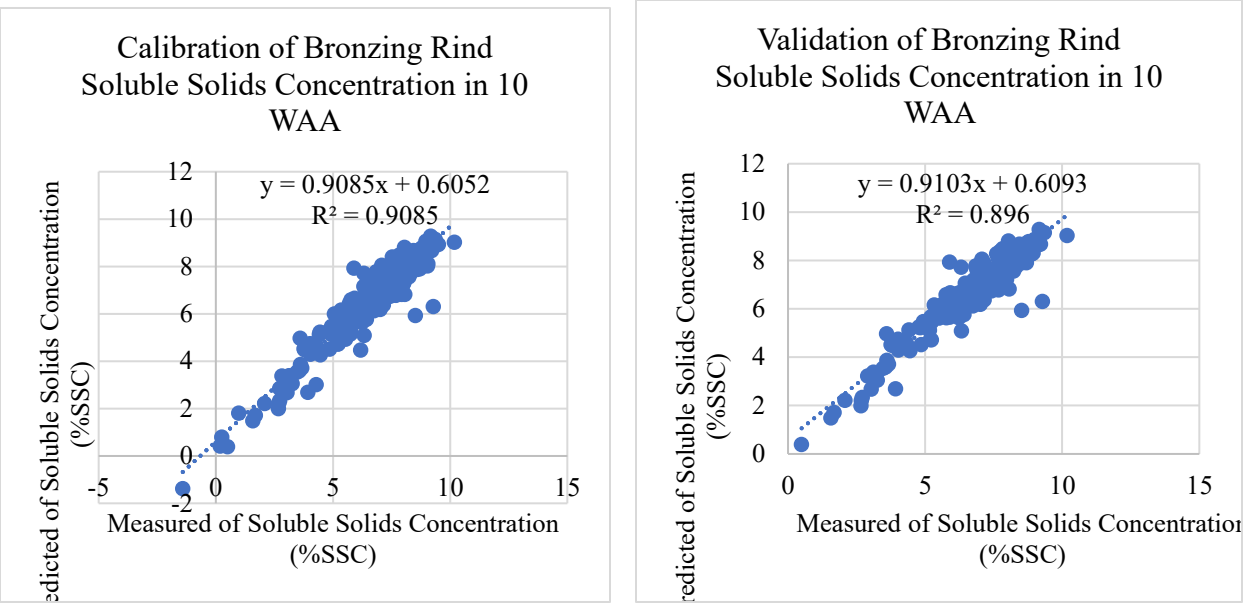

Figure 11: Calibration and validation of bronzing rind soluble solids concentration in 10 WAA

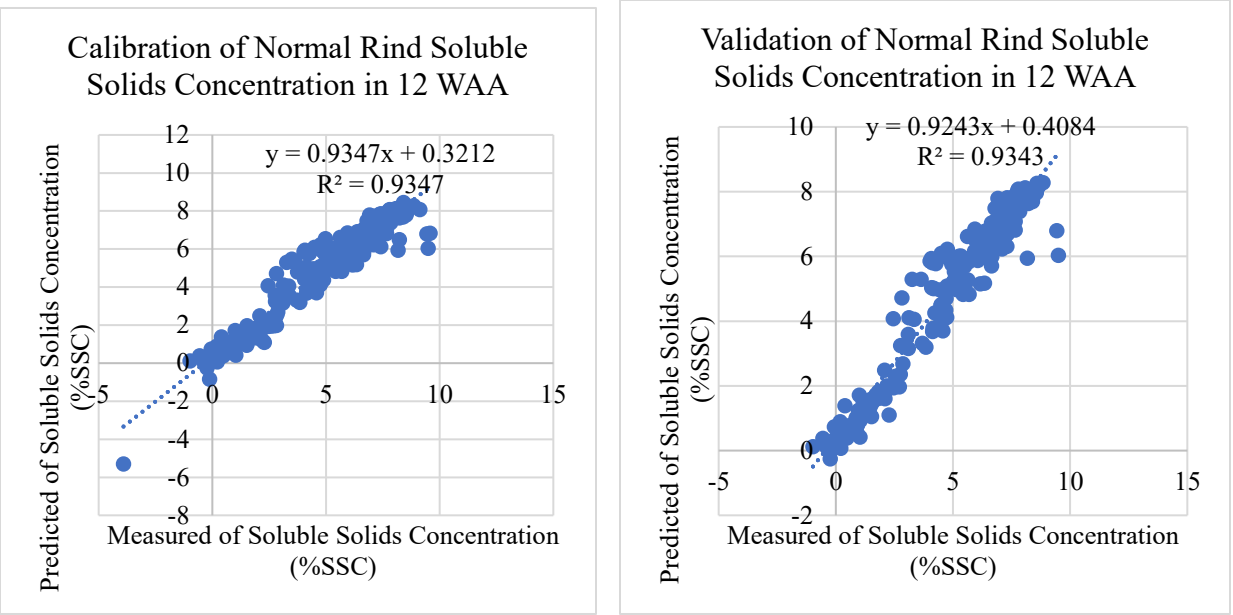

Figure 12: Calibration and validation of normal rind soluble solids concentration in 12 WAA

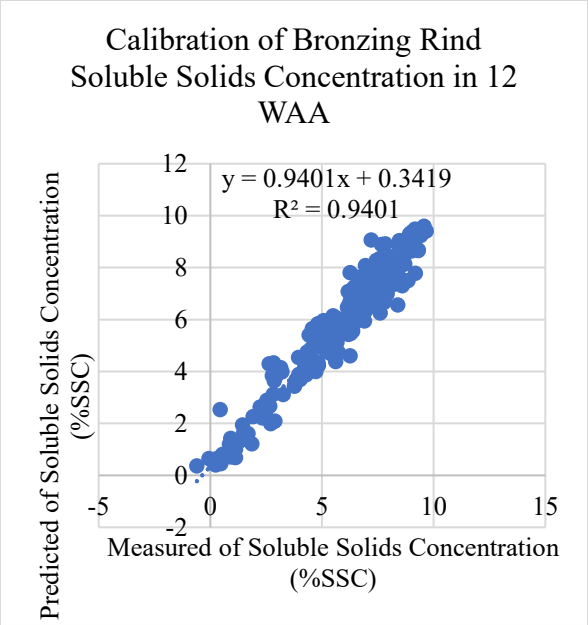

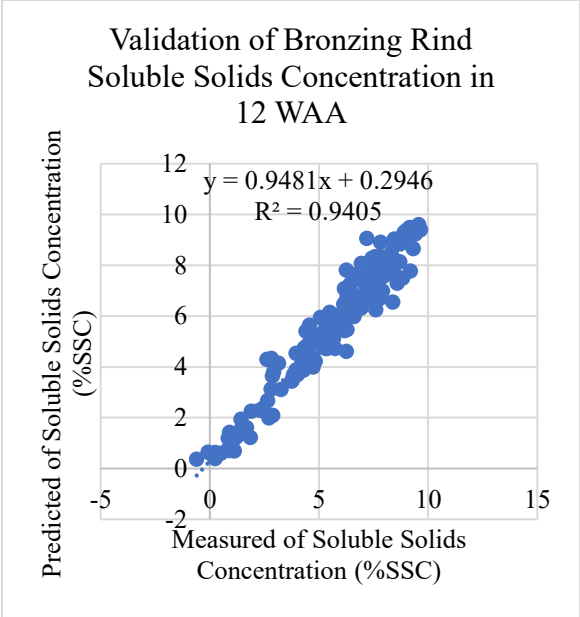

Figure 13: Calibration and validation of bronzing rind soluble solids concentration in 12 WAA

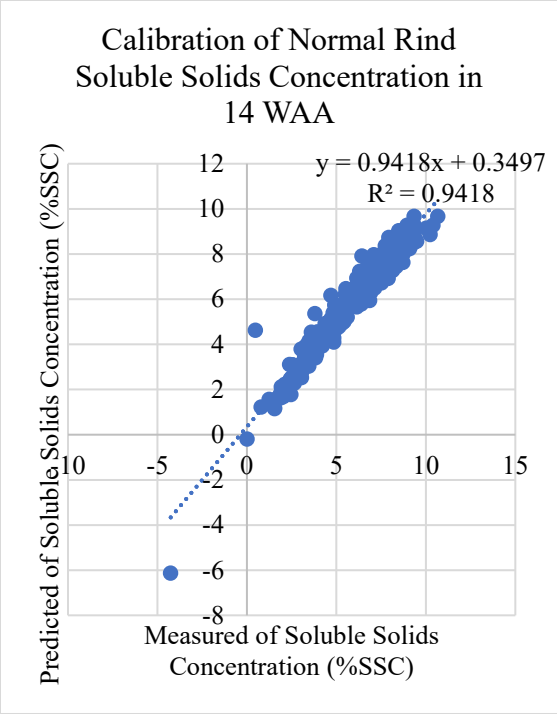

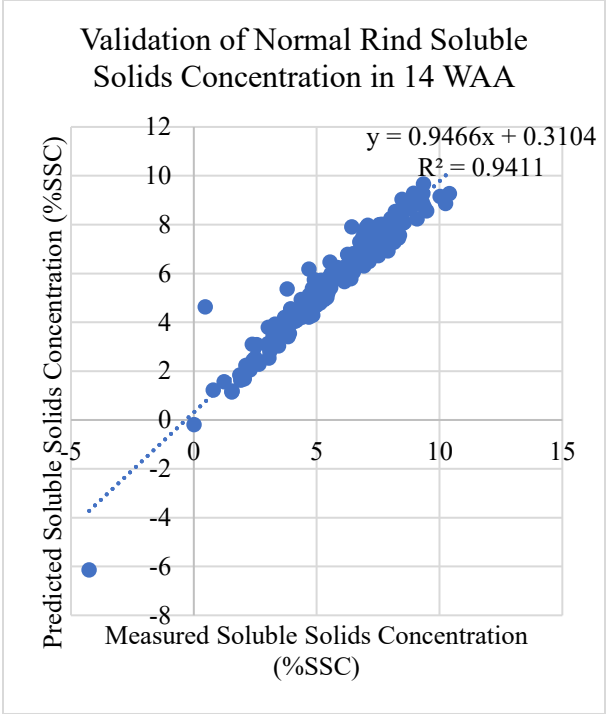

Figure 14: Calibration and validation of normal rind soluble solids concentration in 14 WAA

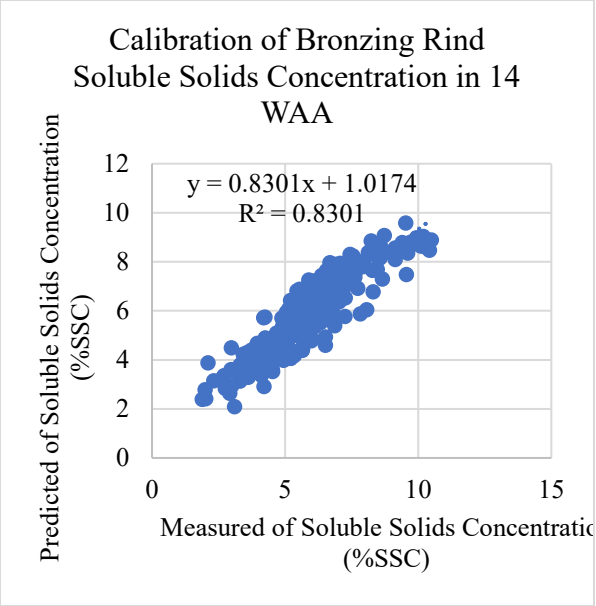

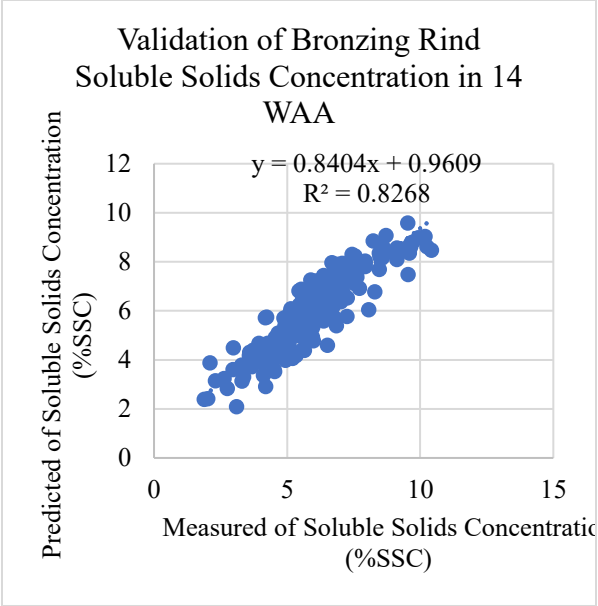

Figure 15: Calibration and validation of bronzing rind soluble solids concentration in 14 WAA

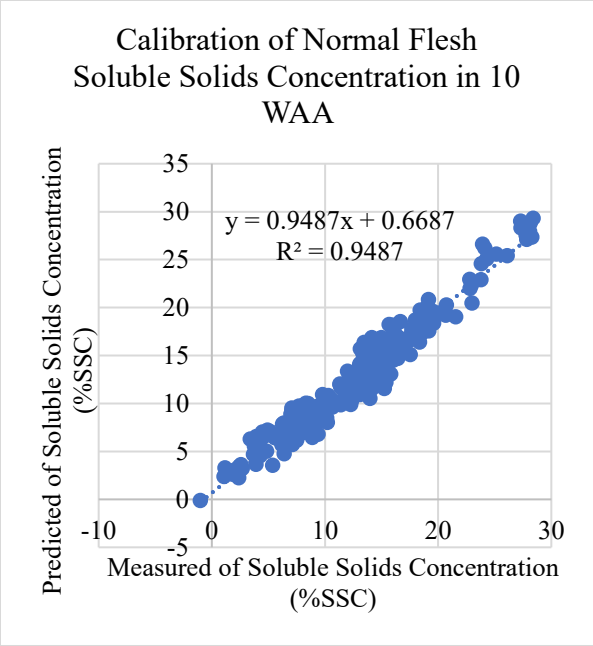

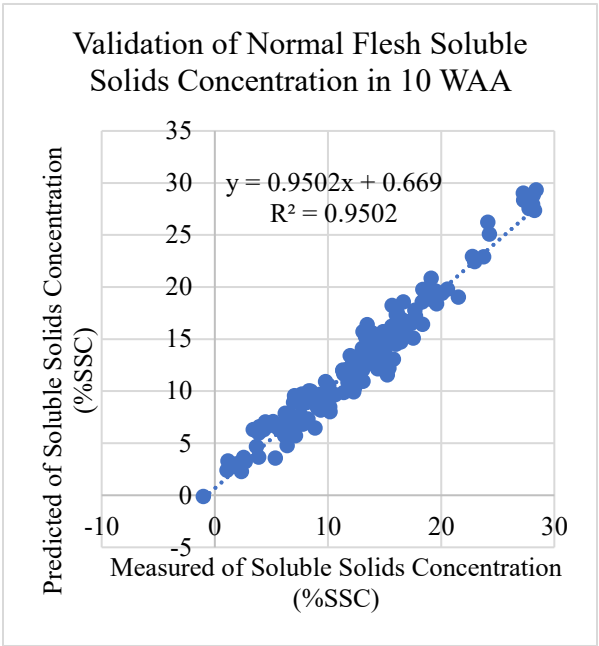

Figure 16: Calibration and validation of normal flesh soluble solids concentration in 10 WAA

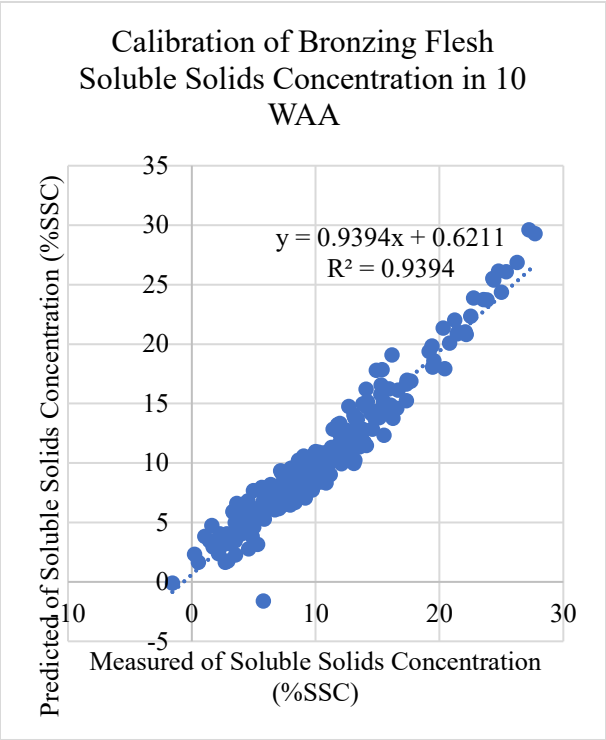

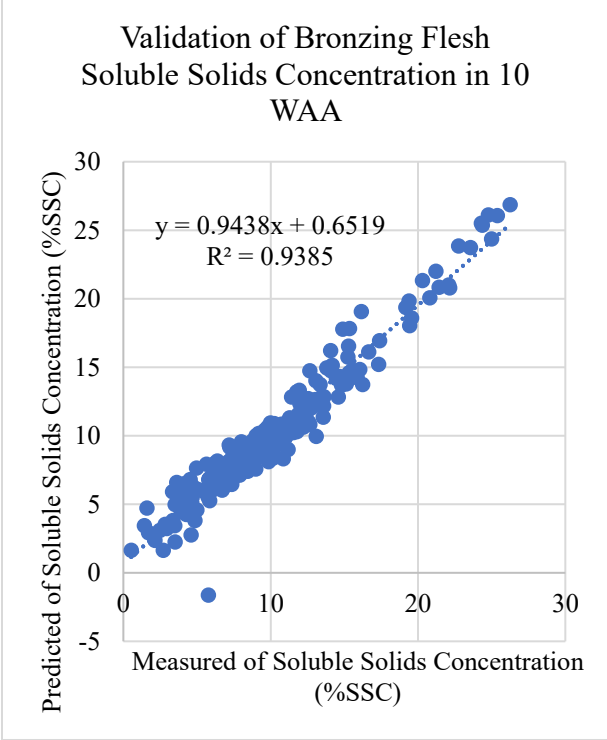

Figure 17: Calibration and validation of bronzing flesh soluble solids concentration in 10 WAA

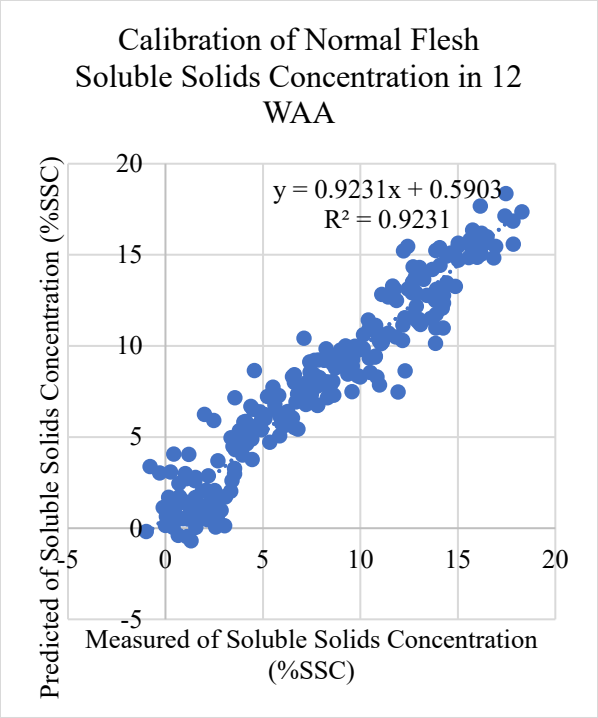

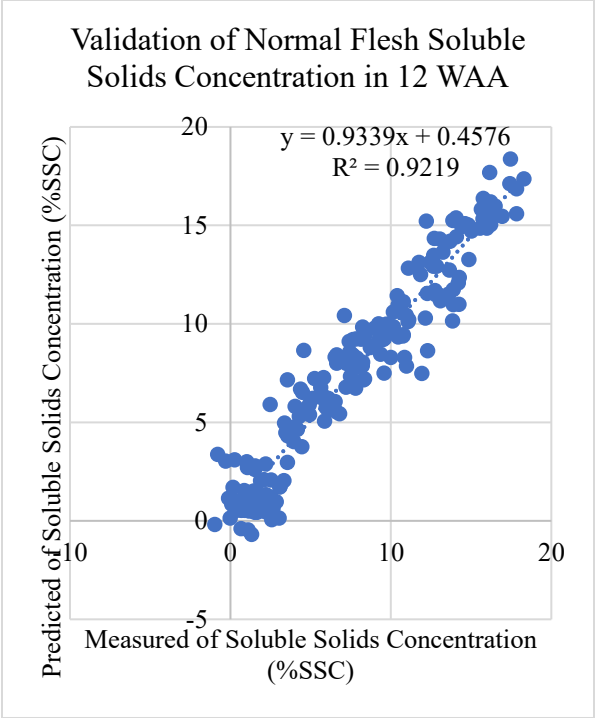

Figure 18: Calibration and validation of normal flesh soluble solids concentration in 12 WAA

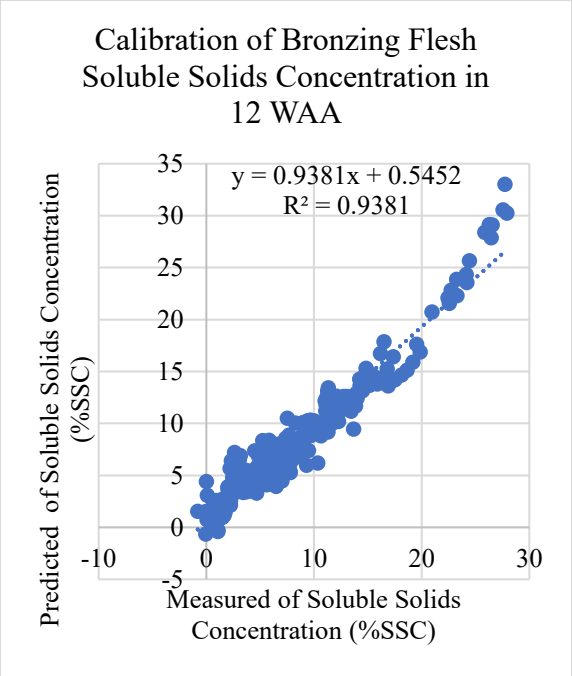

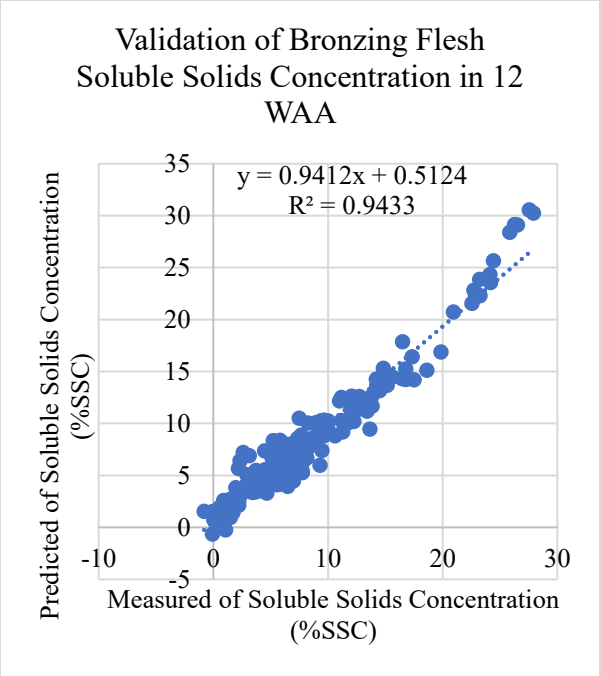

Figure 19: Calibration and validation of bronzing flesh soluble solids concentration in 12 WAA

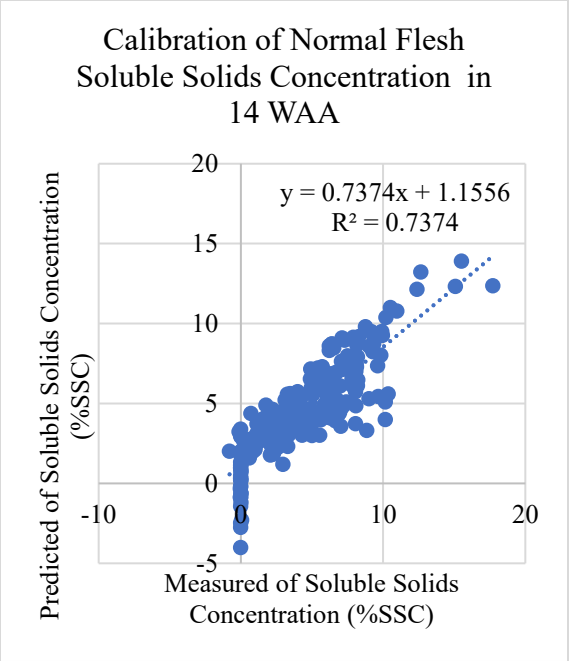

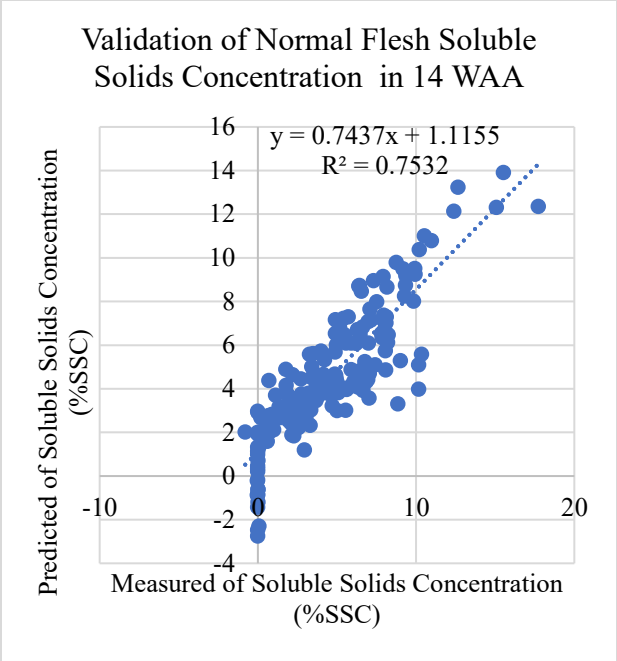

Figure 20: Calibration and validation of normal flesh soluble solids concentration in 14 WAA

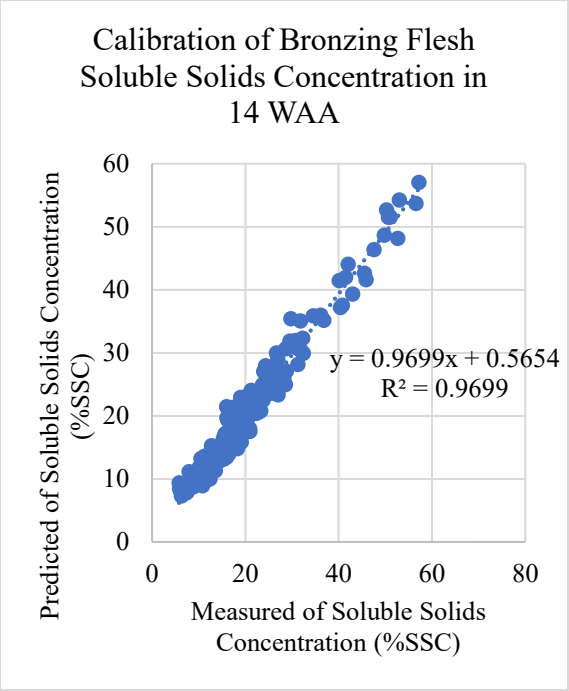

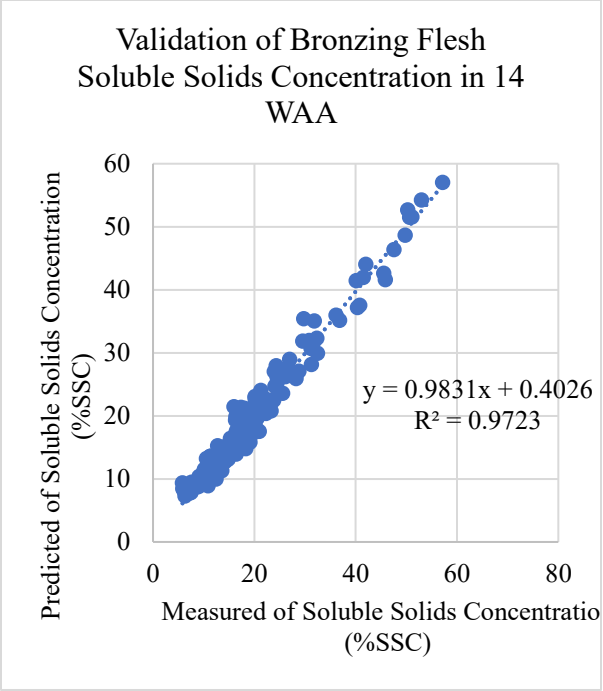

Figure 21: Calibration and validation of bronzing flesh soluble solids concentration in 14 WAA

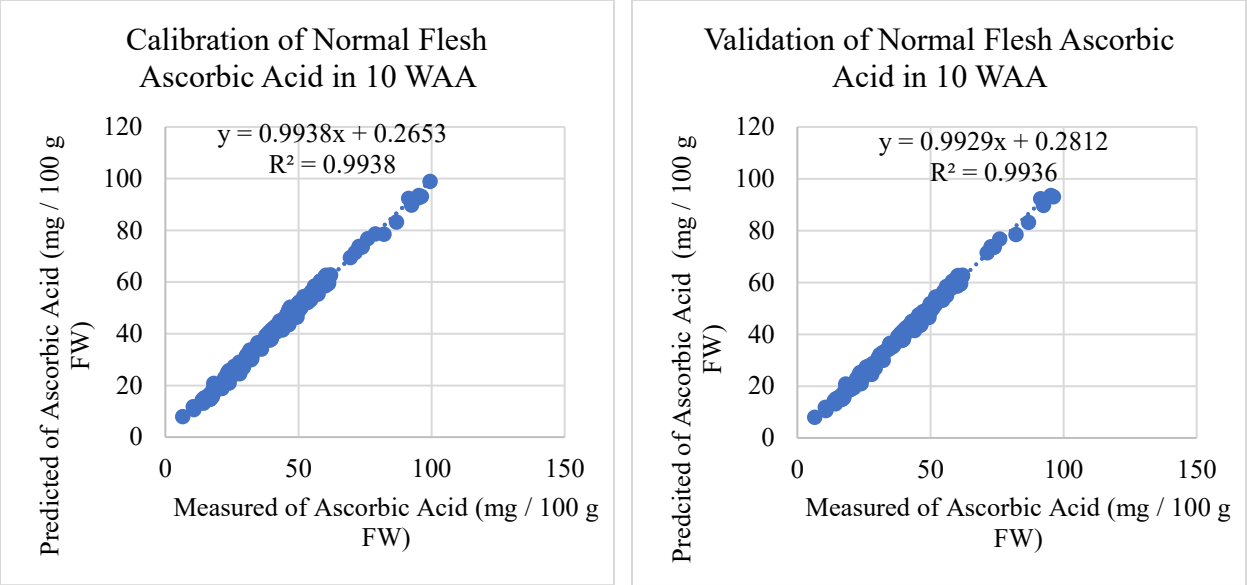

Figure 22: Calibration and validation of normal flesh ascorbic acid in 10 WAA

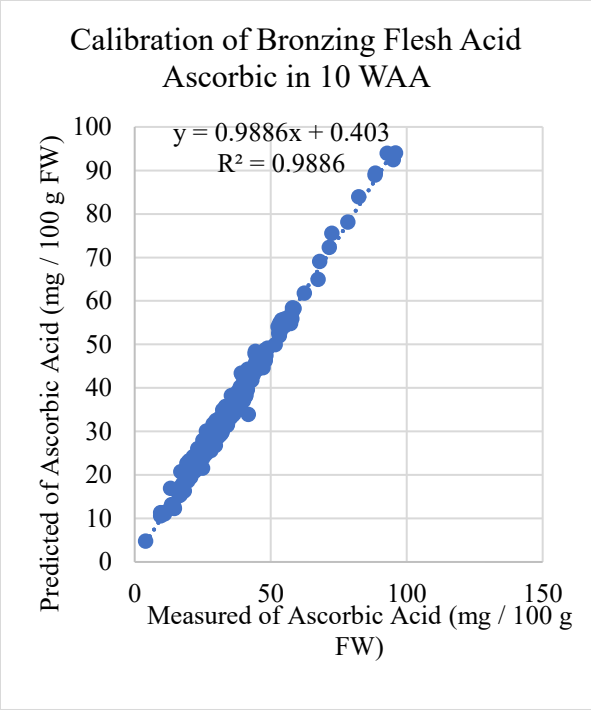

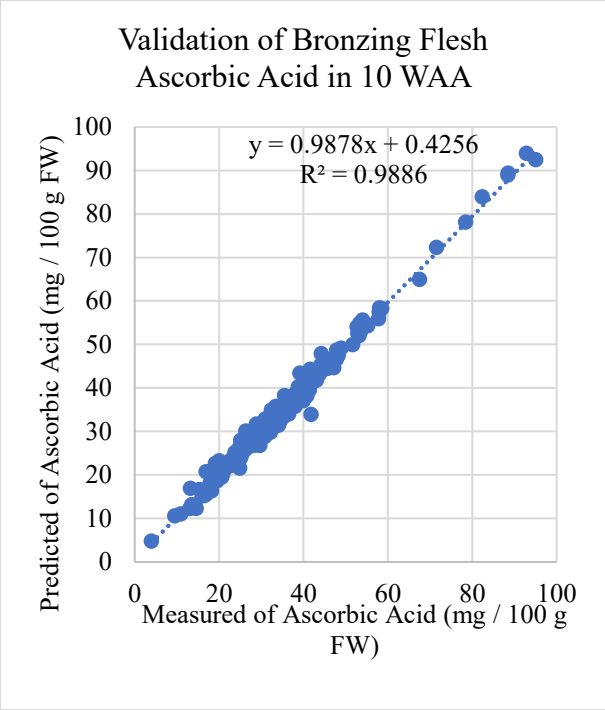

Figure 23: Calibration and validation of bronzing flesh ascorbic acid in 10 WAA

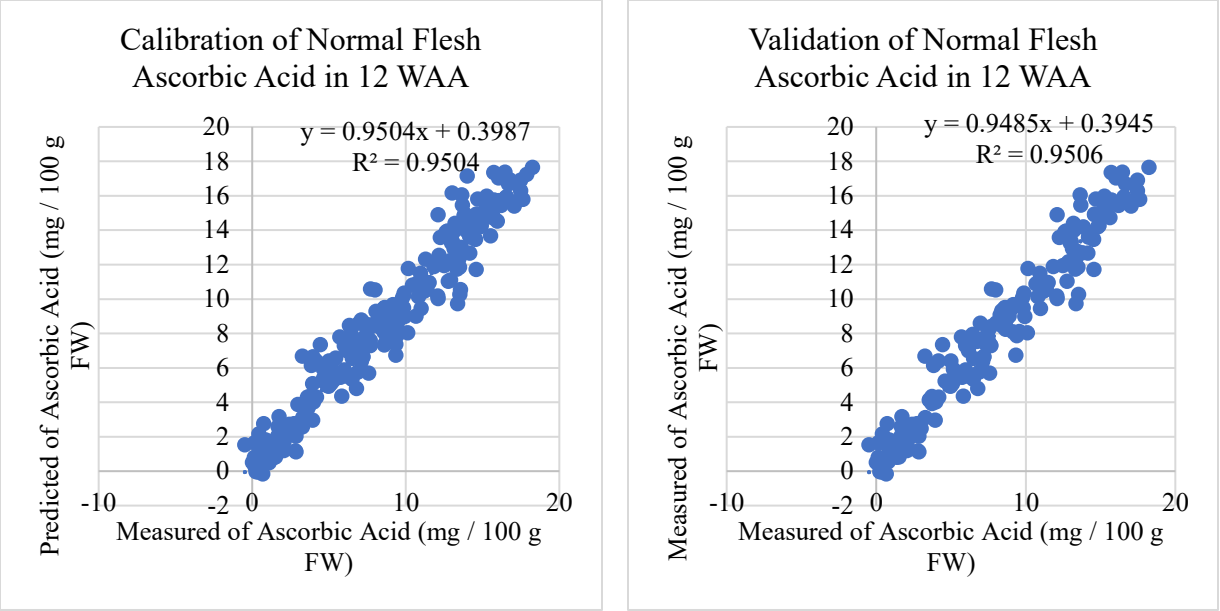

Figure 24: Calibration and validation of normal flesh ascorbic acid in 12 WAA

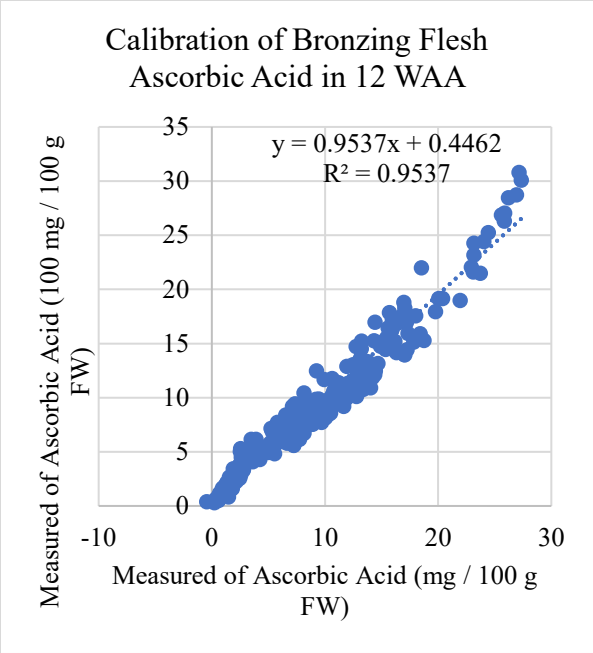

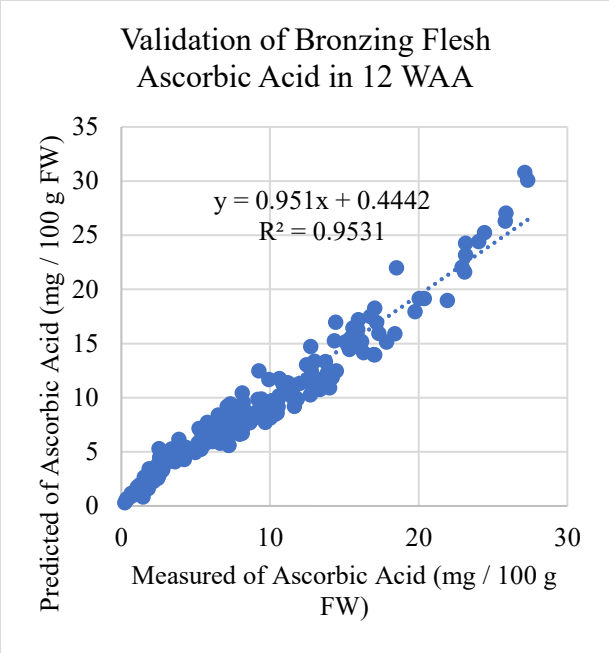

Figure 25: Calibration and validation of bronzing flesh ascorbic acid in 12 WAA

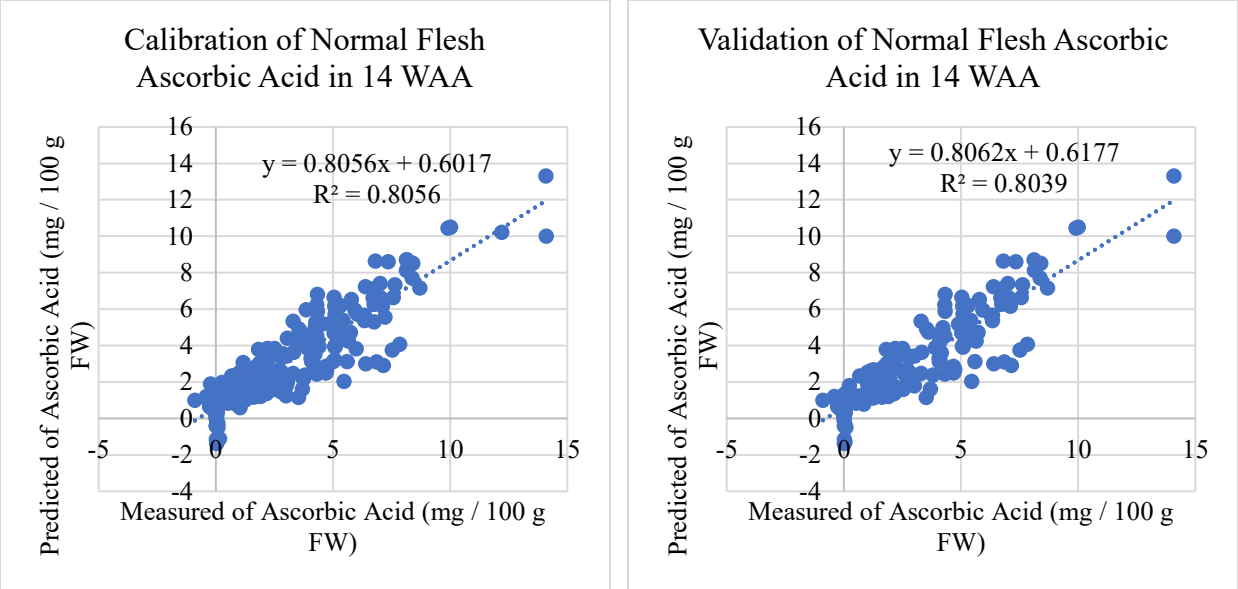

Figure 26: Calibration and validation of normal flesh ascorbic acid in 14 WAA

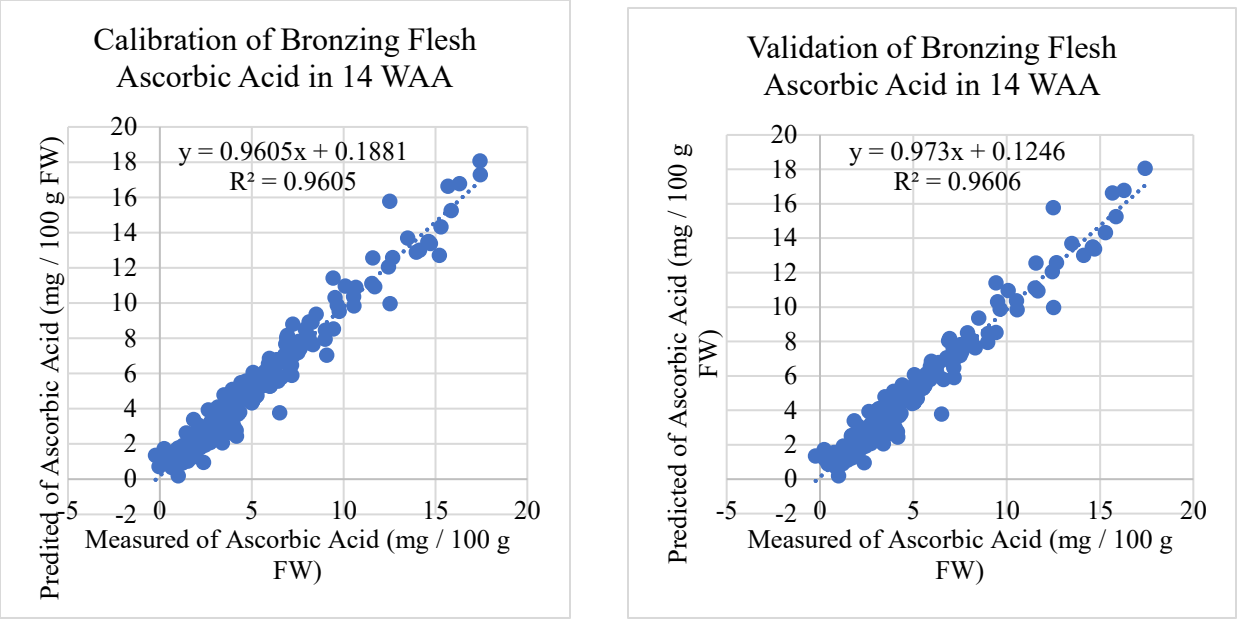

Figure 27: Calibration and validation of bronzing flesh ascorbic acid in 14 WAA